POLITECNICO DI TORINO

Department of Energy

Master's Degree Thesis in Energy and Nuclear Engineering

Synthesis and characterization of Graphene Oxide-doped hydrogels for carbon dioxide capture and sequestration

Supervisors

Prof. MARCO SIMONETTI

Prof. MICHAEL BOZLAR

Candidate

FABIO MARGIOTTA

NOVEMBER 2024

Summary

The scientific research unanimously indicates that anthropogenic carbon dioxide emissions are driving significant and concerning changes in our planet's climate, necessitating immediate action. The deployment of reliable renewable energy systems as well as Carbon Capture and Storage (CCS) technologies is therefore imperative, serving as a crucial interim solution.

This thesis investigates the synthesis and characterization of graphene-based hydrogels for CO_2 capture purposes. Graphene has been widely demonstrated to be an extraordinary material due to its ability to improve most of the properties of host constituents. Its reactivity was upgraded by introducing functional groups, developing Graphene Oxide (GO)-based hydrogels, synthesized through a redox-initiated radical polymerization method by incorporating acrylamide with potassium persulfate (KPS) and Tetramethylethylenediamine (TMEDA), whose combined utilization leads to a fast polymerization executed at room temperature. Adsorption tests were then conducted inside an airtight polycarbonate vessel, which was constructed and precisely tested at the university lab. GO and GO COOH-based gels underwent a functionalization with various amino groups, aiming at enhancing mechanical properties, such as self-healing features, CO_2 adsorption capacities, and efficiencies.

Acknowledgements

Table of Contents

List of Tables

List of Figures

List of abbreviations

GHGs
: Greenhouse Gases

PPM
: Parts Per Million

PPB
: Parts Per Billion

GWP
: Global Warming Potential

AR
: Assessment Report

ERF
: Effective Radiative Forcing

IPCC
: Intergovernmental Panel on Climate Change

CDR
: Carbon Direct Removal

CCS
: Carbon Capture & Storage

DAC
: Direct Air Capture

DFT

Density Functional Theory

AM

Acrylamide

PAM

Polyacrylamide

TRL

Technology Readiness Level

MEA

Monoethanolamine

DEA

Diethanolamine

SAs

Solid Adsorbents

ACs

Activated Carbons

MOFs

Metal Organic Frameworks

AA

Acrylic Acid

GO

Graphene Oxide

rGO

reduced Graphene Oxide

GO COOH

Carboxylated Graphene Oxide

NFG

Natural Flake Graphite

KPS

Potassium Persulfate

TMEDA

Tetramethylethylenediamine

CA

Citric Acid

FTIR

Fourier Transform Infrared Spectroscopy

DSC

Differential Scanning Calorimetry

TGA

Thermo-Gravimetric Analysis

ABS

Acrylonitrile Butadiene Styrene

EDA

Ethylenediamine

BAPA

Bis(3- aminopropyl)amine

TSA

Temperature Swing Adsorption

PSA

Pressure Swing Adsorption

VSA

Vacuum Swing Adsorption

Chapter 1

Introduction

1.1 Motivation

It is undeniable that anthropogenic activities have warmed the atmosphere, land, and ocean over the past two centuries. Scientific evidence indicates that greenhouse gases (GHGs) concentrations have increased in the atmosphere, reaching annual averages of 421 parts per million (ppm) of carbon dioxide (CO_2), 1921 parts per billion (ppb) of methane (CH_4), and 337 ppb of nitrous oxide (N_2O) [1].

Climate change is due to the redistribution of carbon among the so-called carbon pools, which essentially are carbon reservoirs with the capacity to absorb and release carbon. They are able to exchange carbon with one another, employing carbon fluxes, which comprise what is known as the global Carbon cycle. There are five broad global carbon pools, with respective carbon distributions:

1. Atmosphere: 800 Gt
2. Hydrosphere: 40 000 Gt
3. Biosphere: 2500 Gt
4. Lithosphere: 65 000 000 Gt
5. Anthroposphere: With an estimated 2-3 Gt of carbon in the form of fuels, fertilizers, and polymers

While natural exchanges between the first three pools are in the order of 100 Gt C/year, GHG anthropogenic emissions are only 10 Gt C/year, but sufficient to disrupt carbon balance and to change GHG concentrations in the atmosphere [2].

This data refers to the mass of carbon alone in the emitted gases. Since the molar mass of CO_2 is 44 g/mol and includes oxygen atoms bonded with carbon, each

tonne of carbon corresponds roughly to 3.67 tonnes of CO_2. Using this conversion, 10 Gt C/year translates to 36,7 Gt CO_2/year.

However, emissions can also be quantified as tonnes of CO_2-equivalents (CO_{2_eq}), which try to sum all of the warming impacts of the different greenhouse gases together to give a single measure of total greenhouse gas emissions. To convert non-CO_2 gases into their carbon dioxide-equivalents, their mass is multiplied by their global warming potential (GWP), which measures the warming impacts of a gas compared to the reference CO_2. It estimates the "strength" of the greenhouse gas over a 100-year standard time horizon (GWP-100), following the IPCC Sixth Assessment Report (AR6) [3], whose synthesis report was released in 2023.

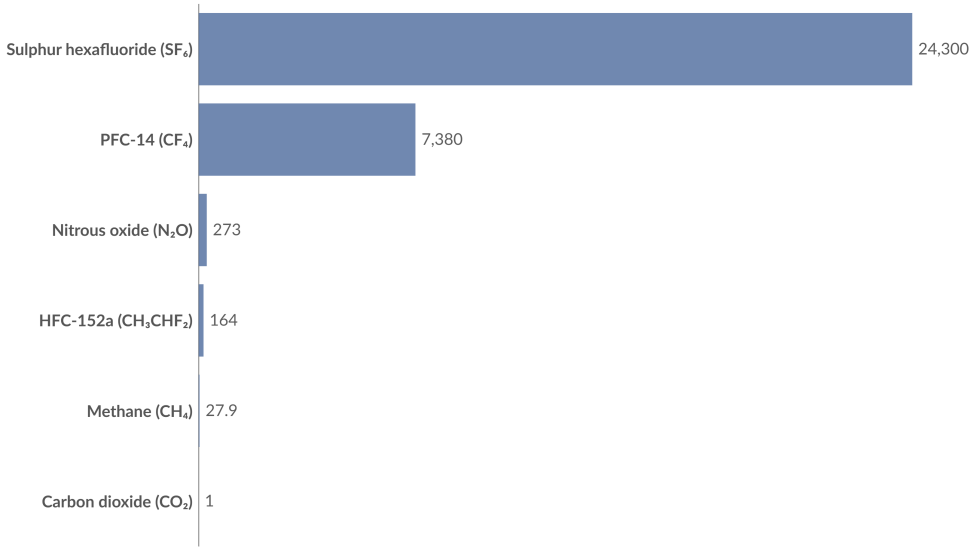

Figure 1.1: Global warming potential of greenhouse gases over 100-year timescale.

By considering the GWP of each greenhouse gas, as visible from the figure 1.1, 50 billion tonnes of GHGs are emitted each year globally in terms of CO_{2_eq}.

Depending on their GWP, all GHGs contribute differently to the Effective Radiative Forcing (ERF), which is used to quantify the change in the energy balance in the Earth's atmosphere, in terms of incoming solar radiation and outgoing infrared radiation. Chapter 7 of IPCC Assessment Report 6 [4] states that the total anthropogenic ERF over the industrial era, from 1750 to 2019, was 2,72 W/m^2, increased by +0,43 W/m^2 from 2011. Anthropogenic emissions of greenhouse gases and their precursors contribute to an ERF of 3,84 W/m^2 over the industrial era, from 1750 to 2019. Most of it comes from carbon dioxide (2,16 W/m^2), methane (0,54 W/m^2), and nitrous oxide (0,21 W/m^2). Ozone's contribution to the ERF is 0,47 W/m^2.

In the context of Radiative Forcing:

- A positive ERF means that the Earth receives more incoming energy from sunlight than it radiates to space, as this gain will cause *Global warming*. The main contributors are GHGs, which trap heat in the atmosphere;

- A negative ERF means that the Earth loses more energy to space than it receives from the Sun, producing *Global dimming*. This is achieved sulfate Aerosols and SO_X, which increase cloud reflectivity, reducing the amount of solar energy reaching and warming the surface.

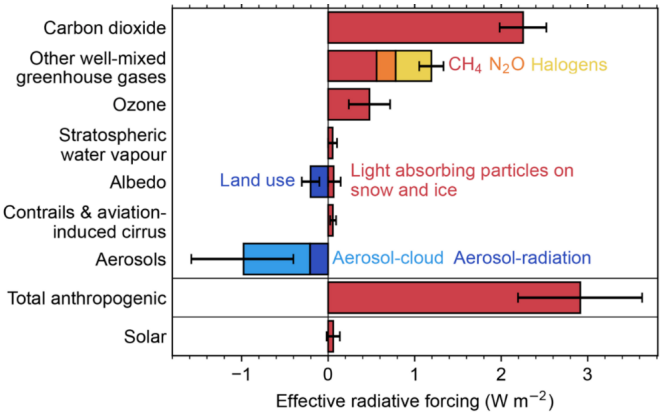

Figure 1.2: ERF assessment from 1750 to 2022.

The IPCC estimates that the human-caused global surface temperature increase from 1850–1900 to 2010–2019 likely ranges between 0.8°C to 1.3°C [5]. The history of global temperature change can be summarized in the figure 1.3.

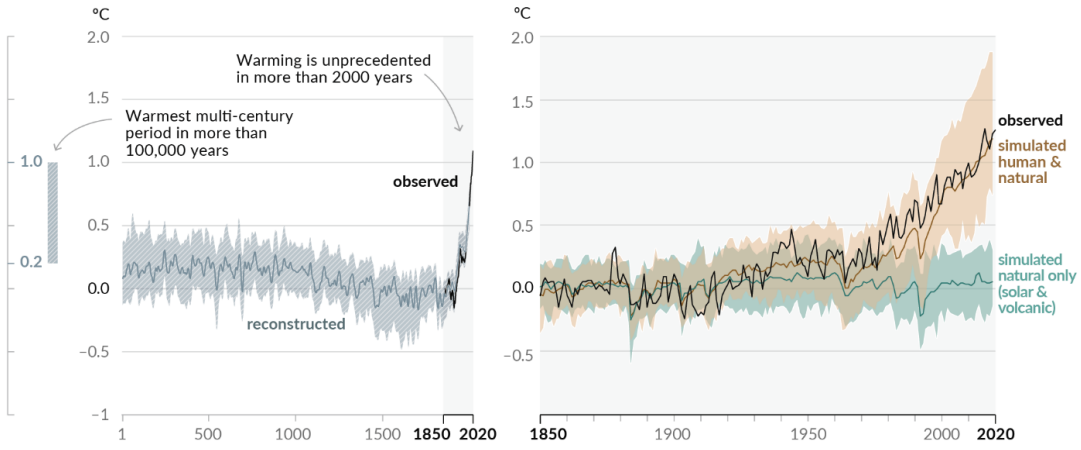

Figure 1.3: Global temperature change and causes.

The IPCC quantifies the impact of greenhouse gases in terms of temperature increase/decrease after 100 years from the emission pulse. Therefore, one pulse of emissions emitted today will generate a certain temperature impact 100 years from now. Focusing at the delayed impact rather than the immediate one is essential as GHGs and pollutants have a certain lifetime in the atmosphere once emitted. For instance, CO_2 has the most remarkable impact because it is the longest-living gas in the atmosphere among the various GHGs included in the IPCC simulation, displayed in the figure 1.4 displayed below.

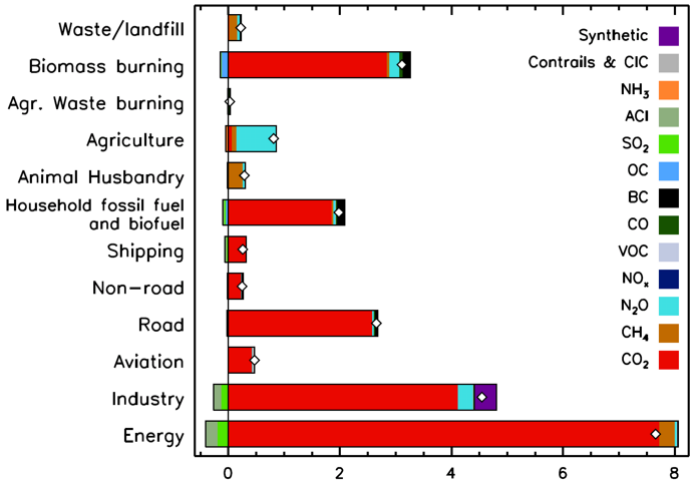

Figure 1.4: GHGs temperature impact at 100 years [mK] by sector.

The cumulated impact of those greenhouse gases can be estimated to be around 25 - 30 mK/year.

Under all emissions scenarios considered, global surface temperature is projected to increase until at least mid-century. Global warming of 1.5°C and 2°C will be exceeded during the 21st century unless deep reductions in CO_2 and other GHG emissions occur in the coming decades.

Compared to 1850-1900 and the respective emission scenario, global surface temperature averaged over 2081-2100 will likely be higher:

- Very low GHG emission scenario: From +1°C to 1,8°C
- Intermediate GHG emission scenario: From 2,1°C to 3,5°C
- Very high GHG emission scenario: From 3,3°C to 5,5°C

The last global surface temperature increase of over 2,5°C was reached over three million years ago.

Climate change, whether driven by natural or human forces, can lead to changes in the likelihood of the frequency, intensity, and strength of extreme weather and climate events such as hot extremes, marine heatwaves, heavy precipitation, and agricultural droughts.

The probability of occurrence of climate or weather events can be described by a probability density function (PDF) and displayed as a Gaussian curve, which can vary its shape in terms of mean, variance, or both, as shown below:

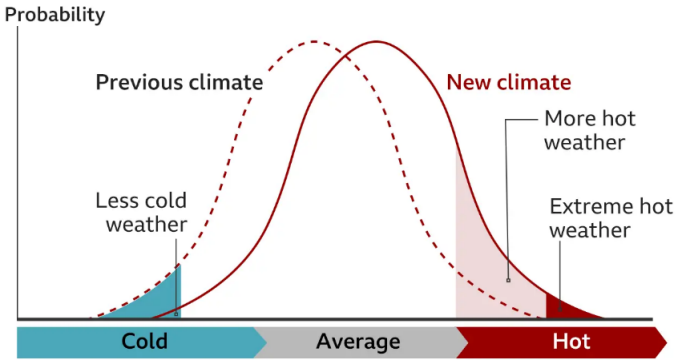

Figure 1.5: Probability density function of daily temperature.

The climate crisis is already affecting inhabited regions across the planet, increasing the average global temperature and leading to heat waves more frequently. The assessment of the observed change and natural consequences, which generate a shift in the geographical distribution of climate zones, can be represented as follows [3]:

- Hot extremes:

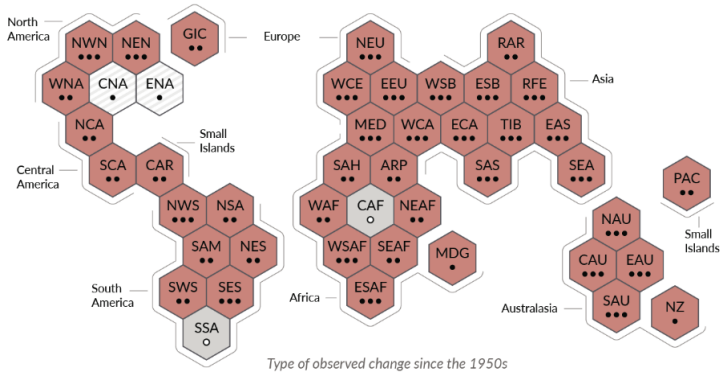

Figure 1.6: Observed change in heat waves in world's regions.

- Heavy precipitation:

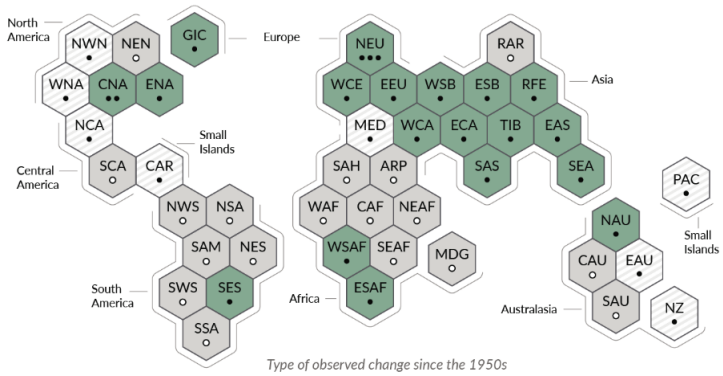

Figure 1.7: Observed change in precipitations in world's regions.

- Agricultural droughts:

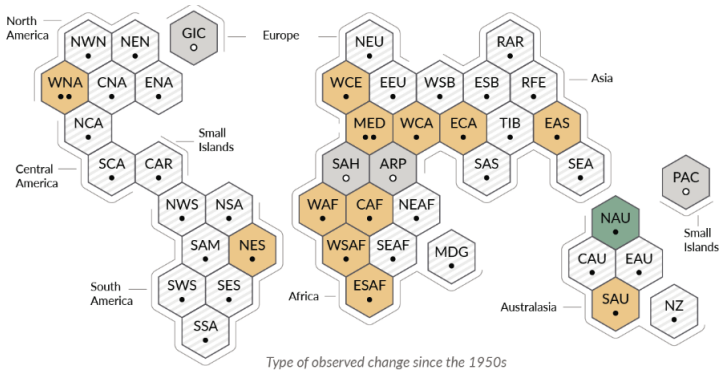

Figure 1.8: Observed change in droughts in world's regions.

Inhabited world regions are displayed as equally sized-hexagons. The colors represent the outcomes of the assessment, whereas the human confidence level contributing to the observed changes is expressed through dots, as low (•), medium (• •), or high (• • •).

Following these consequences, in addition to rising sea levels, desertification, natural disasters, and the pressure of pollution and loss of habitat, the annual average displacement risk is constantly rising in the most affected areas of the globe, such as South Asia, Latin America, and Africa, leading to the migration of the so-called Environmental Refugees, forced to flee their communities and expected to reach around 1,2 billion by 2050 [6].

1.2 Scope of the thesis

This work aims to evaluate the main carbon capture and storage (CCS) techniques, as they represent one of the most efficient ways to reduce the emissions of carbon dioxide in the environment, focusing on the synthesis and applications of hydrogels.

Specifically, it will follow an investigation into the effects of functional groups on graphene oxide, employing computational techniques, such as the Density Functional Theory (DFT) method, which is essential to explore the electronic structure of atoms, molecules, and condensed phases.

The primary objective of the thesis is the characterization and comparison of different types of Polyacrylamide (PAM) hydrogels, which differ depending on the various ratios of graphene oxide and amino groups employed. Analytical techniques and experimental adsorption tests have been carried out to quantify their performance.

1.3 Thesis structure

The entire study has been divided into five different chapters, which are summarized here below:

1. Introduction: Overview of climate change basics, explaining what topic is being studied and why;

2. Fundamentals: A literature review of current CCS principles, most deployed approaches, and basics on the definition and structure of hydrogels, attempting to identify gaps that this research will aim to fill;

3. Method: Summary of useful chemical compounds as well as techniques and general rules that have been followed to synthesize graphene oxide and hydrogels;

4. Results: Evaluation of the registered performances following 24h adsorption tests, performed inside an airtight polycarbonate container, and mechanical tests, to measure the ultimate tensile strength and self-healing properties;

5. Conclusion and future outlook: Study limitations and optional fields of applications of PAM hydrogels.

Chapter 2

Fundamentals

2.1 Carbon capture and sequestration principles

In order to determine how emissions can be most effectively reduced and what can and cannot be eliminated with current technologies, a breakdown scheme is needed to consider hard-to-abate sectors and processes that mostly account for them.

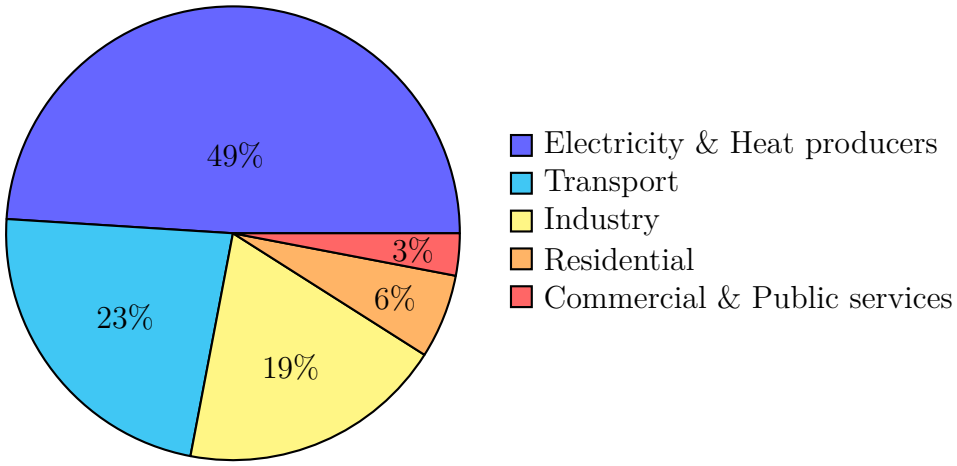

Figure 2.1: Global greenhouse gas emissions by sector [7].

As of 2022, global CO_2 emissions were 34 billion tonnes, whereas all greenhouse gas emissions could be quantified as 49 billion CO_2eq [7][8].

It is evident that primary sources of GHGs come from electricity and heat generation, since electricity mostly comes from burning fossil fuels, such as coal, which accounted for over 75% of those emissions, oil and natural gas. It is essential to incentivize and invest in increasing the efficiency of fossil-fired power plants and shifting generation from higher-emitting to lower-emitting, possibly substituting

coal with natural gas.

Concerning the transportation sector, about 94% of the fuel is petroleum-based, which includes gasoline and diesel, making this sector the largest source of direct emissions and the second largest of indirect ones. Opportunities to reduce emissions in this sector mostly rely on fuel switching, reduction of travel demand, and improvements in fuel efficiency, design, and operating practices.

The last major driver is the industry sector. Greenhouse gas emissions, which are linked to chemical reactions necessary to form goods from raw materials, are split into two categories: direct (produced within the facility) and indirect (which occur off-site to power buildings and machinery). The European Union Emission Trading System (EU ETS) introduced a Cap & Trade scheme which brought the industry sector emissions down by 35% between 2005, when it was established, and 2019. The drop target has been raised to 62% to be achieved by 2030 [9].

Stopping global warming requires net greenhouse gas emissions to fall to zero and remain at zero thereafter. To achieve that, greenhouse gas emissions must terminate. However, scientific research and literature are concluding that rapid emissions drop to remain within a 1,5°C temperature rise above pre-industrial levels is practically impossible at the moment. Therefore, the implementation of reliable carbon dioxide reduction strategies is imperative, since it represents a key interim solution to permanently remove CO_2 from the atmosphere to put the energy sector on a sustainable path.

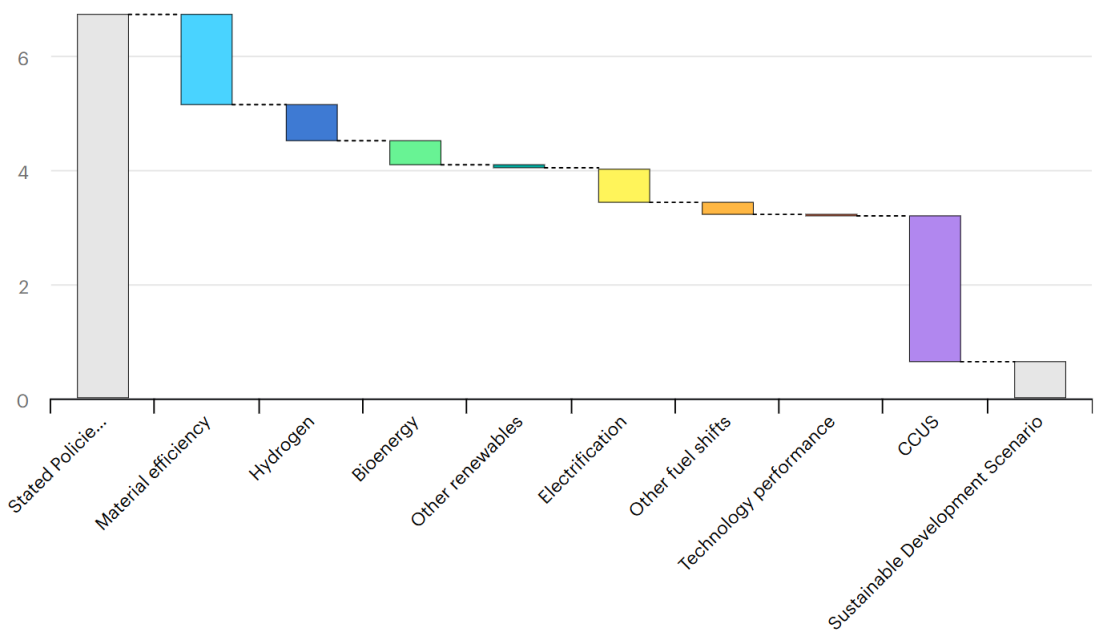

Figure 2.2: Global CO2 emissions reductions in $GtCO_2$ in the heavy industry by mitigation strategy, [10].

Main carbon capture technologies can be executed through different methodologies:

1. Carbon Direct Removal (CDR): It aims at actively removing carbon dioxide from the atmosphere to use or store it in some way through the following strategies:
    - Direct Air Capture (DAC): It directly removes carbon dioxide from the atmosphere by using a large fan to blow ambient air through a vent into a collector, where CO_2 sticks to a filter;
    - Afforestation and Reforestation: By planting more trees which can act as carbon sinks, by utilizing the natural process of photosynthesis;
    - Bioenergy with Carbon Capture and Storage (BECCS): Involving capture and storage of CO_2 from processes where biomass gets converted into fuel;
    - Ocean Fertilization: Achieved by adding nutrients to the surface of the ocean to stimulate photosynthesis by phytoplankton;
    - Biochar Carbon Removal (BCR): A stable form of carbon, known as biocarbon, produced via pyrolysis and applied in agriculture for generations to improve soil quality. It is ideal for small-scale applications, such as farmers.
2. Carbon Capture & Storage (CCS): Executed to remove CO_2 from industrial installations, preventing it from entering the atmosphere by acting at the point of emission. This is employed utilizing:
    - Pre-Combustion: Capturing CO_2 before fossil fuels have been burned, usually in coal-gasification plants;
    - Post-Combustion: Most mature application, consisting in capturing CO_2 after fossil fuels have been burned, often in coal-fired or gas-fired processes;
    - Oxyfuel Combustion: By burning fossil fuels with pure oxygen instead of air. In this way, flue gases, mostly made of CO_2 and water vapor, are easier to capture by cooling them down;
    - Chemical Looping Combustion (CLC): It uses metal oxides, made of iron, copper, or nickel, to transfer oxygen to the fuel, separating the combustion process into two distinct steps. This allows for nearly pure CO_2 capture without the need for additional separation processes.

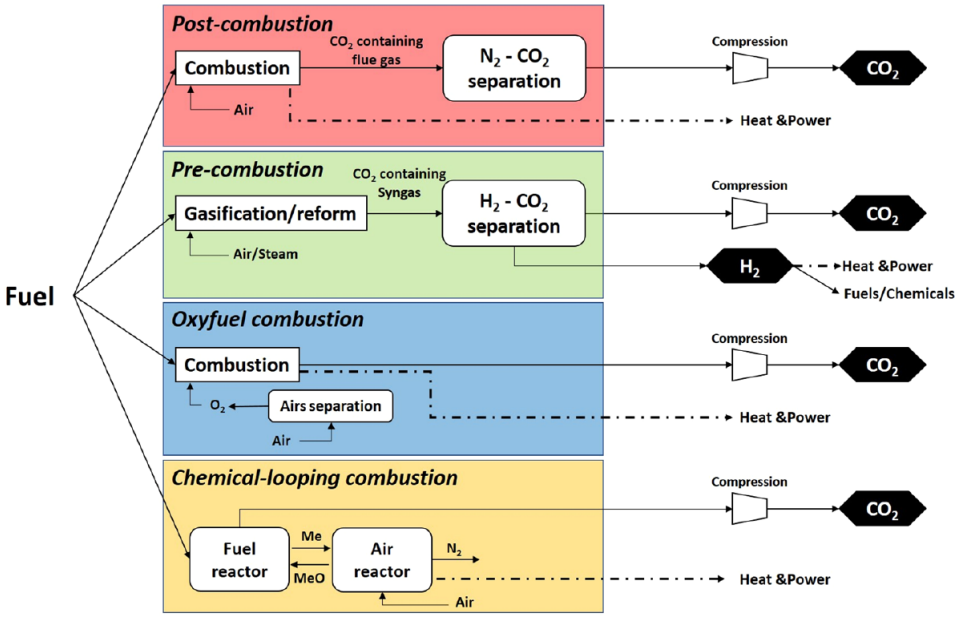

Figure 2.3: Schematic representation of CCS systems, [11].

2.2 Mature approches

The essential drivers of CCS strategies deployment include several factors:

- Policies and regulatory frameworks
- Economics of scale
- Technological innovation
- Energy security
- Utilization of capture CO_2 (CCUS)
- Energy costs

Mature and emerging technologies are being surveyed depending on their Technology Readiness Level (TRL).

The isolation of carbon dioxide from flue gases can then be achieved through four different separation strategies:

Technology	Mechanism	Advantages	Disadvantages
Absorption	Mass transfer of particles into another substance	High efficiency, most mature process	Sorbent degradation, dependence on CO_2 concentration
Adsorption	Adhesion of particles over a solid sorbent	Reversible process, adsorbent recyclability	High energy requirement for CO_2 desorption
Membrane separation	Selective transport and separation through membranes, driven by pressure difference	High separation efficiency	Low fluxes and fouling
Cryogenic distillation	Desublimation (from vapor to solid ice) under low-temperature conditions	Solid CO_2 melted to high-purity liquid ready for transport	Energy-intensive, viable for high CO_2 concentration

Table 2.1: Comparison of different separation technologies, [12][13].

Despite the importance of CCUS for achieving clean energy transitions, the implementation has been slow to take off. It is a technology that can only be implemented on stationary sources, such as power plants and industrial applications, which account for 50% of the total emissions, while the other half of them is related to transportation. Moreover, only a few countries have a price associated with the emissions of CO_2, and as long as it can be emitted for free, there is little if any economic incentive for CCS. In addition, the large-scale storage of carbon dioxide in geological formations raises concern about the safety of this process for the public. The IEA quantifies around 20 commercial CCS operations worldwide, with more than 30 new CCS facilities to be announced in recent years [14].

Several factors can justify the slow uptake of CCS strategies, but the high expenditure is one of the most frequently heard, arguably making it unable to compete with wind and solar electricity given their impressive fall in costs over the last decade.

Among the three steps constituting the CCS process (Capture, Transportation, and Storage), capture makes up the most energetically demanding, accounting for about 70-80% of the total cost [15]. Of this penalty about 30% is the energy required to compress CO_2 and 70% of the energy is used for the separation of CO_2 from flue gases.

Generally, carbon capture applications do not showcase the same cost, as visible in the figure below:

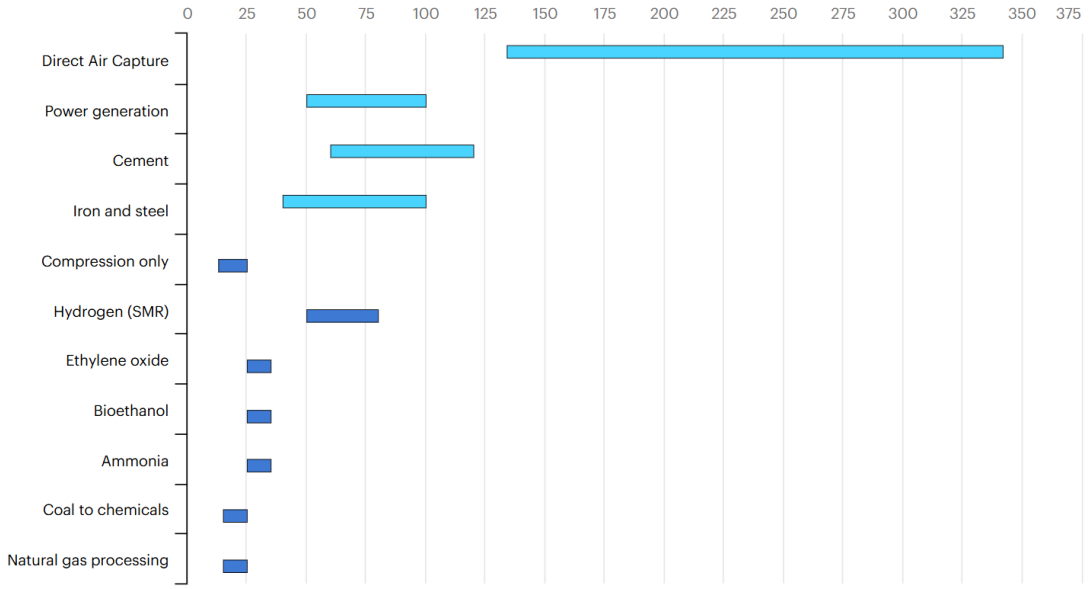

Figure 2.4: Levelized cost of CO_2 capture by sector in USD/tonne, [14].

CCS strategies are among the cheapest abatement options from the industry point of view since they are relatively advanced and cost-competitive for drastically cutting their emissions.

For instance, by considering the industrial production of ammonia, which is used as a fertilizer, the employment of CO_2 capture on traditional natural gas-based plants leads to a 20-40% increase in the estimated costs, whereas the conversion of the plant into hydrogen routes would result in a 50-115% rise on costs [14]. This proves that carbon capture applications can be equipped on existing coal and gas-fired plants to provide capacity and supply of electricity anytime with no intermittency, which is different from conventional solar and wind options.

Cost reductions have already been achieved, as large-scale CCUS projects in the power sector have dropped by 35% due to market evolution and expansion.

Typically, every technology development progresses through a series of scale-up steps, such as Laboratory, Pilot, Demo, and Commercial scales.

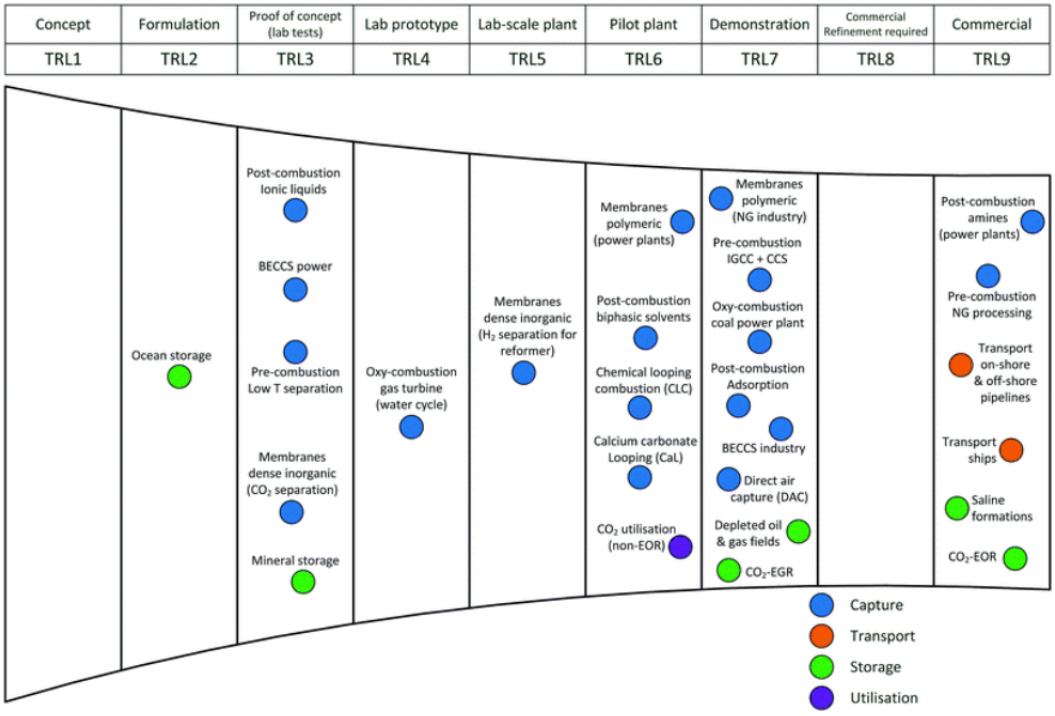

Figure 2.5: Development progress of different CCS technologies on a TRL scale, [16].

Post-combustion flue gases exiting a power plant vary according to different factors, such as the type of fuel burned. For instance, coal-fired power plant exhausts typically showcase a composition of 12% CO_2 + 88% N_2, with traces of H_2O, O_2, NO_x, and SO_x. On the other hand, natural gas-fired power plants exhibit a lower CO_2 content (3-7%), while oil-fired plants have similar values to the coal ones, between 10 and 15%.

Therefore, an ideal carbon capture material would feature a high selectivity of CO_2 over the other flue gases, high volumetric CO_2 adsorption capacities, long-term stability, and rapid diffusion of the gas through the adsorbent material.

The most mature absorption capture approach (TRL 9) involves the utilization of Aqueous amine solutions, such as Monoethanolamine (MEA), Diethanolamine (DEA), and Potassium carbonate for post-combustion exhaust gases, with efficiency of over 90%. Although amines are considered a state-of-the-art material for CO_2 capture, they are energy-intensive, prone to equipment corrosion, and lack stability [17].

There is a high need for new and more effective materials that reduce energy requirements, minimize environmental impact, and offer efficient CO_2 uptake. Among the alternative solutions, Piperazine ($C_4H_{10}O_2$), with TRL 5-7, stands

out due to its superior CO_2 absorption, enhanced kinetics, and lower energy requirements.

Ionic liquids (TRL 2-4), which also perform absorption, are gaining interest due to their peculiar characteristics, such as tunability, negligible vapor pressure, wide liquid range, thermal stability, and reduced corrosiveness compared to traditional Amine-based solutions. Nonetheless, these alternatives still showcase several drawbacks: Piperazine exhibits higher corrosiveness and toxicity, while Ionic liquids tend to be highly viscous, costly, and less efficient in terms of capture capacity.

Alternatively from traditional methods of scrubbing with liquid amines, CCS can be carried through adsorption processes, with a capacity of solid adsorbents (SAs) of around 3 mmol/g. Due to cost-effective steps, low regeneration energy requirement, and ease of applicability over a wide range of pressures and temperatures, the adsorption method of capture is found to be the most appealing approach [18]. Furthermore, SAs have demonstrated the ability to substantially reduce the capital and operating costs for CCS [19].

Overall, most of the physisorbents exhibit low CO_2 uptakes at low pressures and low selectivity, but the adsorbent material can be regenerated by a simple change in either temperature or pressure.

In the case of chemisorption, carbon dioxide reacts with the sorbent surface via covalent bonding. However, the regeneration of adsorbents is quite challenging, making it an energy-intensive process.

In contrast to liquid adsorbents, SAs over a wide range of temperatures have been reported in the literature for both chemi/physisorption as promising materials since they are less toxic, less corrosive, and with better CO_2 capture efficiency with respect to amines. They also appear to be easy to handle and can be recovered back for the next cycle by varying pressure, temperature, or by vacuum. This approach leads to a significant reduction in both capital and operating costs for CCS. SAs can be found in the form of carbonaceous materials including Activated Carbons (ACs), Modified Silica, Graphene, Zeolites, and Alkali-based adsorbents.

Porous crystalline materials, such as metal-organic frameworks (MOFs) and covalent organic frameworks (COFs) (both TRL 4-6) have gathered significant attention due to their high surface area, tunable properties, low regeneration energy requirements, and sensitivity to humid environments. Unfortunately, these materials face challenges including long-term stability issues, high manufacturing costs, and difficult scaling up process.

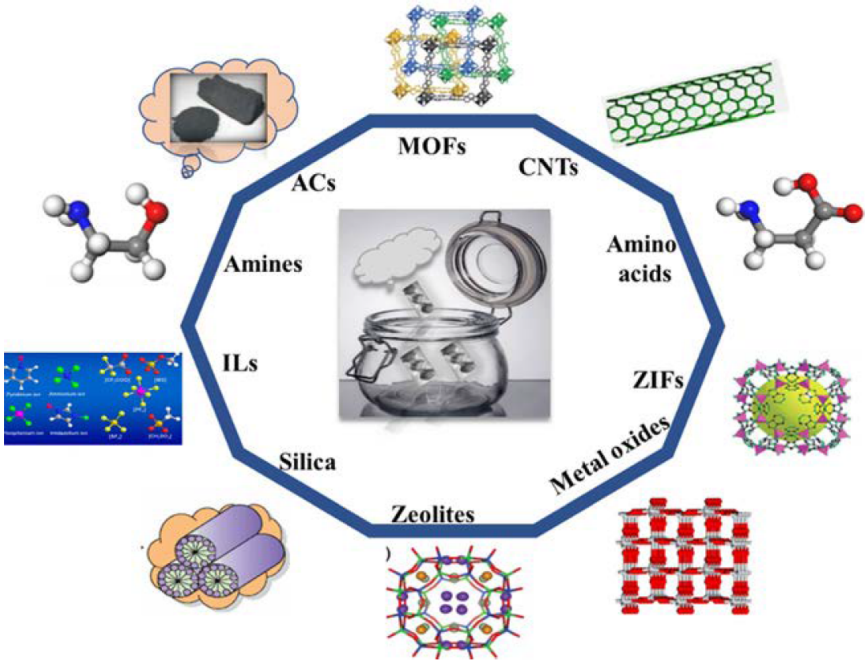

Figure 2.6: List of solid adsorbents studied in the literature for CCS, [18].

Lastly, polymeric membranes (TRL 7-8), such as Polaris™, represent a promising technology for mitigating CO_2 emissions due to their simplicity, compactness, low-energy requirements, and cost-effectiveness. They can perform carbon capture through selective separation, driven by permeation rather than pure adsorption or absorption, by allowing the selective transport of certain gases based on differences in solubility and diffusion rates through the membrane material. Nonetheless, a membrane with simultaneously high stability, selectivity, and flux is not yet available in today's market.

It is important to note that a tough challenge in the implementation of all these carbon capture technologies is the presence of impurities and defects in the gas stream that can poison or even damage the absorber. The performance of adsorbents is usually quantified depending on their selectivity, adsorption capacity, economical regeneration process, and high stability.

2.3 Hydrogels

Hydrogels are a group of water-swellable polymeric materials produced by a single reaction of one or more monomers. They show a hydrophilic structure that makes them capable of holding enormous amounts of water in a three-dimensional network, up to 1000 times the mass of the polymer [20], filling the space between macromolecules. Their ability to absorb water derives from hydrophilic functional groups attached to the polymeric backbone, such as -COOH, -NH_2, and -OH, whereas their resistance to dissolution comes from cross-links between network chains.

They are developed from:

- Natural polymers: Available in nature, such as gelatin and collagen;
- Synthetic polymers: From polymer groups that are hydrophobic in nature, such as polyacrylamide and polyvinyl alcohol;
- A combination of both.

Natural hydrogels are being replaced by synthetic ones due to their enhanced performance, such as a longer service life, higher capacity of adsorption, short degradation rate, and more strength.

They are also classified according to [21]:

1. Number of monomer species: Homopolymeric, copolymeric, and multipolymeric;
2. Configuration: Amorphous, semi-crystalline, and crystalline;
3. Type of cross-linking: Chemical, physical;
4. Network electrical charge: Nonionic, ionic;
5. Physical appearance: Matrix, microsphere, film.

Hydrogel production can be carried out in two ways [22]:

- Physical cross-linking: Formed by non-covalent bonds, such as hydrogen bonds, ionic interactions, and Van der Waals forces. They are reversible, meaning that the gel can be disrupted and modified by tuning temperature or pH. This results in a low mechanical strength and stability;
- Chemical cross-linking: Consisting of covalent bonds through a cross-linking agent or free radical polymerization. The final structure is permanent, making the gel more robust and less likely to dissolve, with high stability and durability.

Chemically cross-linked hydrogel production usually features a reaction between hydrophilic monomers and functional cross-linkers, with the addition of radical initiators, able to produce free radicals by light or heat exposure. Dilutes, such as water, can be added to control the final properties. The polymerization can be initiated thermally by UV irradiation or a redox initiator system.

These versatile materials showcase limited mechanical properties in their native state [23] but offer significant tunability through cross-linking strategies [24]. Nanocomposite and chemically enhanced hydrogels demonstrate superior mechanical performance, enabling applications in diverse fields such as drug delivery systems, electronics, sensors, and energy storage.

Thus, the utilization of hydrogels for CO_2 capture represents a novel and promising approach in this field. Chemical modification and functionalization of hydrogels, such as the one with Graphene and Graphene Oxide (GO), are auspicious strategies that could overcome the limitations of plain hydrogels and previous sorbent materials.

The mechanism of CCS in hydrogels typically involves physical absorption and chemical interactions, such as hydrogen bonding and coordination with amine or other reactive groups within the hydrogel matrix [25]. These interactions facilitate the efficient capture and storage, positioning hydrogels as a viable component in CO_2 capture technologies.

The most common monomers in industrial production are Acrylic Acid (AA) and Acrylamide (AM). Each of them contains a carbon double bond from which an active center may propagate to produce a polymer chain.

In the case of AM, acrylamide monomers react through a cross-linking effect to form long chains of Polyacrylamide (PAM), which is a synthetic polymer. Polyacrylamide-based hydrogels are one of the most common options, as they exhibit substantial volume transition in response to chemical or physical stimuli, appearing to be non-toxic, stable, and non-resorbable sterile watery gels [20].

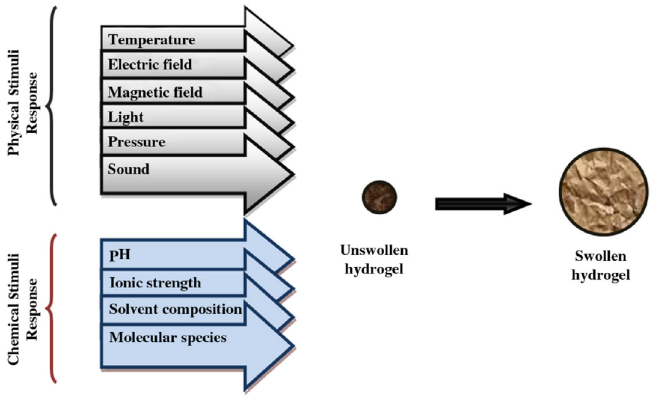

Figure 2.7: Stimuli response swelling hydrogel, [21].

Chapter 3

Method

3.1 Chemicals

Several varieties of materials have been employed for the synthesis and development of both graphene and PAM-based hydrogels during the next steps of this study. All useful chemicals can be listed and summarized in the table 3.1 below:

Element	Provider
Natural flake graphite [1] (400 μm)	Asbury Carbons
Potassium permanganate $KMnO_4$ (99%)	Alfa Aesar
Sulfuric acid H_2SO_4 (95-98%) Hydrochloric acid HCl (37%) Phosphoric acid H_3PO_4 (85%) Nitric acid HNO_3 (65%) Chloroacetic acid $ClCH_2CO_2H$ (99%) Citric acid $C_6H_8O_7$ (99,5%) Ethanol C_2H_6O (99,5%) Sodium hydroxide $NaOH$ (98%) Acrylamide C_3H_5NO (99,9%)	Fisher Chemical
Bis(3-aminopropyl)amine $C_6H_{17}N_3$ (98%) Tetramethylethylenediamine (TMEDA) $C_6H_{16}N_2$ (99%) Potassium persulfate (KPS) $K_2S_2O_8$ (99,5%)	Sigma-Aldrich

Table 3.1: List of employed substances to carry out the study.

[1] It is probably the most familiar of the natural graphite materials. As the name suggests, flake graphite has a distinctly flaky or platy morphology, [26].

3.2 Graphene synthesis

As a basal plane of graphite, graphene is a single-atom-thick layer of carbon atoms of a honeycomb structure, arranged in a hexagonal lattice nanostructure. It is considered to be the basis of carbon nanotubes (CNTs), [27]. Therefore, graphite is composed of multiple layers of graphene.

Each atom in a graphene sheet is connected to its three nearest neighbors by σ-bonds [1] and a delocalized π-bond [2], which contributes to a valence band that extends over the whole sheet.

Graphene has quickly shown enormous potential as a multifunctional filler due to its remarkable ability to enhance the mechanical, thermal, electrical, and chemical properties of host materials, [27][28].

However, graphene is chemically inert, making itself unsuitable for carbon capture, and the effects of incorporating it into hydrogels remain largely unexplored, resulting in numerous uncertainties. Thus, its chemical functionalization, obtained by introducing vacancies and functional groups visible in figure 3.2, has been used for a wide range of applications and is recently being explored to improve the selectivity and absorptivity of CO_2 molecules for CCS purposes, [29].

With the intention of increasing the chemical reactivity towards carbon dioxide, the oxidation of graphite is performed using strong oxidizing agents, introducing oxygenated functionalities in the graphite structure which not only expand the layer separation but also make the material hydrophilic, meaning that they can be dispersed in water [30]. This property enables the graphite oxide to be exfoliated in water through Sonication, ultimately producing single monolayers of graphene, known as graphene oxide (GO), which are just composed of carbon, oxygen, and hydrogen in variable ratios. The main difference between graphite oxide and graphene oxide is, thus, the number of layers.

Overall, one of the most effective ways of synthesizing graphene on a large scale is by the chemical reduction of graphene oxide, generating the so-called Reduced Graphene Oxide (rGO). Common reduction processes include annealing between 200 and 1000°C, as well as hydrothermal, chemical, or electrochemical reduction. Nonetheless, the conductivity of rGO appears to be lower by a factor of 10-100 than the one of pristine graphene [31]. The electrical performance is found to be poorer because of the presence of residual functional groups, remaining after the reduction.

[1] Formed by a head-on overlap of atomic s,p orbitals.

[2] Formed in addition of σ-bonds by sideways overlap of atomic p orbitals.

The most commonly used techniques to synthesize graphite oxide are:

Feature	Brodie (1859)	Staudenmaier (1898)	Hummers (1958)
Oxidizing agents	Fuming nitric acid (HNO_3), potassium chlorate ($KClO_3$)	Concentrated sulfuric acid (H_2SO_4), nitric acid (HNO_3), potassium chlorate ($KClO_3$)	Concentrated sulfuric acid (H_2SO_4), sodium nitrate ($NaNO_3$), potassium permanganate ($KMnO_4$)
Reaction time	Several days	Several days	Few hours
Safety	Hazardous	Hazardous	Safe
Degree of oxidation	High	High	Controlled
Environmental impact	Significant (oxic by-products)	Significant (chlorinated by-products)	Low
Graphene oxide quality	Low (excessive oxidation)	Low (large defects)	High (better control)

Table 3.2: Comparison of main GO synthesis methods.

The traditional Hummers' method was modified and improved in 2013 [32] by oxidizing graphite oxide with potassium permanganate in concentrated sulfuric acid at low temperatures (35°C). The mixture is diluted by slowly adding distilled water dropwise, to ensure a highly qualitative product. Subsequently, the solution is treated by adding water and hydrogen peroxide (30% H_2O_2 solution) to remove sodium nitrate directly in the reaction to prepare the same GO in terms of structure and chemical properties. Graphene oxide is separated through filtration and then washed carefully with acetone. Finally, the precipitate is dried at 80°C under vacuum conditions for 24 hours. This strategy reduces the use of experimental reagents and lowers the cost, making it cheaper and environmentally friendly [33].

The effectiveness of the oxidation method can be assessed by the proportion of graphite oxide in the product or by its carbon-to-oxygen ratio. Well-reacted GO samples will have a C/O ratio between 2,1 and 2,9. Also, the product's color may be used as a criterion for the degree of oxidation. A product rich in graphite oxide will appear bright yellow, whereas poorer samples with higher C/O ratios will have a green-to-black hue, [34].

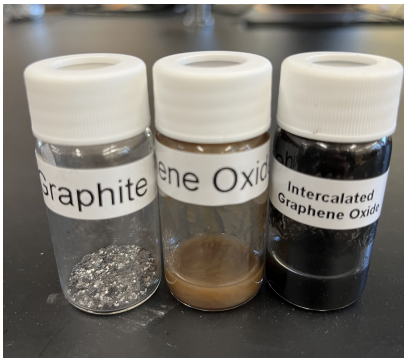

Figure 3.1: Different appearances of samples.

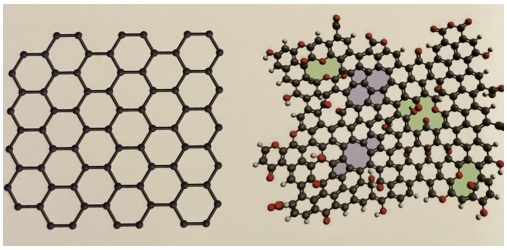

Figure 3.2: Pristine v. functionalized graphene.

A modified Hummer's method was employed in this study to synthesize monolayers of graphene oxide (GO), starting from natural flake graphite (NFG), [35], then adding oxidizing agents, such as sulfuric acid, nitric acid, and potassium permanganate. However, these strong agents often leave residual salts, such as manganese salts or other by-products that can contaminate the final product. Therefore, all impurities were removed by performing a multi-step washing process with hydrochloric acid (3x) and ethanol (3x), followed by repeated deionized water washing to achieve a near-neutral pH.

After each washing cycle, a centrifugation step is executed for 45 minutes at 3500 rpm, aiming to separate the solid part at the bottom from the liquid one at the top, made up of the added acid + impurities.

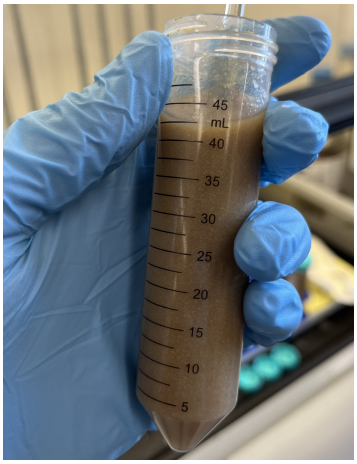

Figure 3.3: Washing process of GO through stirring inside a falcon.

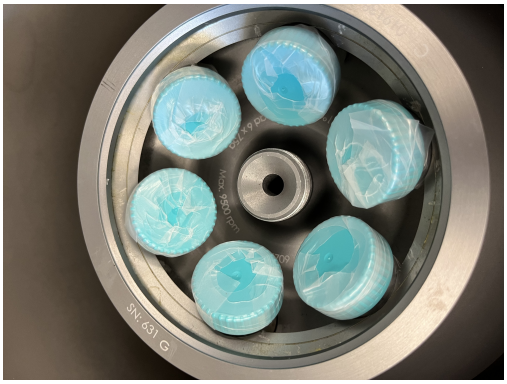

Figure 3.4: Falcons disposal inside a centrifuge.

During the synthesis, the layers of graphene oxide can aggregate due to van der Waals forces and interactions between oxygen-containing functional groups. The multi-step washing process, combined with stirring and centrifugation, helps prevent this aggregation, ensuring the GO remains well-dispersed in solution. This is a crucial point for producing high-quality GO with fewer defects and more consistent properties.

Dry graphene oxide powder was mixed with ultra-pure water in a 1:1 mass ratio to prepare GO dispersions or solutions for the upcoming hydrogel synthesis processes. That ratio of mg to mL is considered to be convenient because it usually provides a balance where the GO sheets can be evenly dispersed without significant aggregation, making the solution homogeneous.

The relatively low-concentration GO suspension is also beneficial in terms of viscosity, helping to easily handle and mix the solution with other reagents. An optimal dispersion of graphene oxide (GO) in water is performed using Sonication, which can convert ultrasonic waves' sound energy into physical vibrations [36], helping to break up any agglomerates or clusters of GO sheets, while ensuring that the GO is evenly dispersed in the solution.

This is feasible as the high-frequency sound waves create microscopic bubbles in the liquid, a process known as Cavitation. When these bubbles collapse, they generate localized shock waves and high shear forces, that are strong enough to break up the aggregates and separate individual GO sheets, leading to a well-dispersed colloidal suspension.

As the duration usually fluctuates between 15 and 45 minutes, the procedure requires the usage of an ice bath to prevent overheating of the solution and protect the integrity of the sample, precluding the glassware from shattering due to thermal stress.

Figure 3.5: Sonicator working at a frequency between 20 and 40 kHz.

Figure 3.6: GO solution.

The adsorption potentiality of graphene oxide can be further enhanced by functionalizing it with Chloroacetic acid ($ClCH_2CO_2H$), which comprises the modification of GO structure by introducing carboxyl functional groups (-COOH). The driving forces for CO_2 adsorption are the electrostatic interactions with hydroxyl and carboxyl groups. Although, carboxyl groups appear to have a higher binding potential than the hydroxyl ones [37], therefore their presence can be tuned to improve the performance of the material for CCS purposes.

Carboxylated graphene oxide (GO-COOH) was prepared by mixing under constant stir two different solutions:

- Solution 1: 50 mg GO + 50 ml ultra-pure water
- Solution 2: 50 ml ultra-pure water + 1,2g $ClCH_2CO_2H$ + 1g NaOH

During the reaction, salt (NaCl) and sodium chloroacetate ($C_2H_2ClNaO_2$) can be released as by-products because of the interaction between chloroacetic acid and sodium hydroxide (strong base).

The pH of the obtained mixture was checked by utilizing a pH paper, which shows a green color when neutrality is achieved. The product GO-COOH was separated through filtration, before being washed with acetone and dried at 80°C for 24 hours. A flow diagram to summarize the key steps is shown in the figure 3.7.

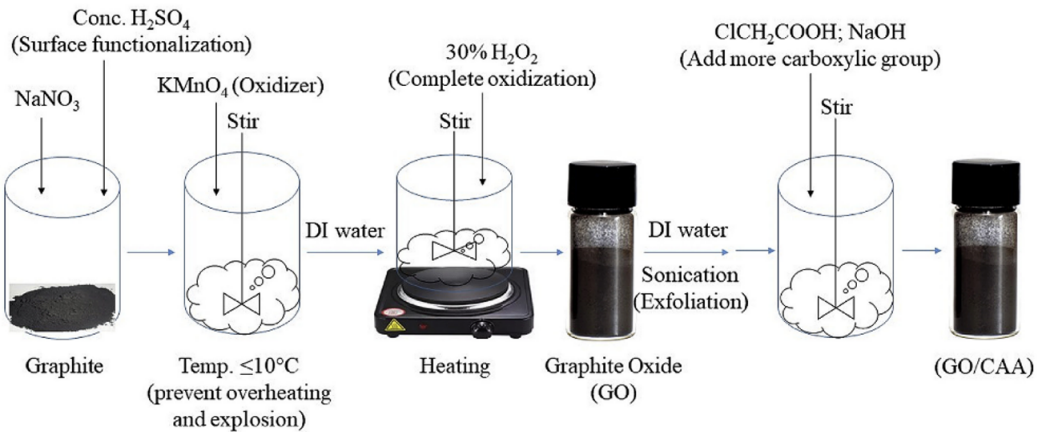

Figure 3.7: Oxydation and carboxylation steps to obtain GO-COOH, [37].

3.3 DFT modelling

The Density Functional Theory (DFT) is a computational quantum-mechanical method that allows the investigation of ground-state properties of condensed matter systems [38].

The first principle DFT calculations are carried out by the QuantumEspresso open-source package [39], where several topics are examined:

- Electronic properties of the material;
- Ground-state configurations;
- Charge density difference;
- Density of states.

Overall, the carbon dioxide capture properties of the two materials can be analyzed and compared with regard to the adsorption energy, whose most common form is [40]:

$$E_{ads} = E_{total} - (E_{substrate} + E_{adsorbate}) \tag{3.1}$$

Where the substrate is either graphene or graphene oxide and the adsorbate is carbon dioxide. Therefore:

$$E_{ads} = E_{G/GO+CO_2} - (E_{G/GO} + E_{CO_2}) \tag{3.2}$$

The adsorption energy E_{ads} of G/GO quantitatively describes the energy changes associated with the adsorption of molecules onto these materials, providing insights into the strength and nature of interactions. Adsorption studies on the most stable GO configuration demonstrated higher adsorption energy compared to pristine graphene, suggesting that the interaction is primarily governed by physisorption. The respective values, measured in electron volts (eV), are shown in the table 3.3. The negative signs indicate that the adsorption process is thermodynamically favorable, resulting in an energy release, demonstrating the interaction of CO_2 molecules onto the surface is more stable and spontaneous than the separation.

Structure	Adsorption energy (eV)
Graphene	-0,16
Graphene oxide	-0,23

Table 3.3: Adsorption energy comparison.

As expected, graphene oxide showcases a higher reactivity and selectivity towards CO_2 molecules than pristine graphene because of its oxygen-containing functional groups (hydroxyls, carboxyls, epoxides), as also visible from the figures 3.8, 3.9.

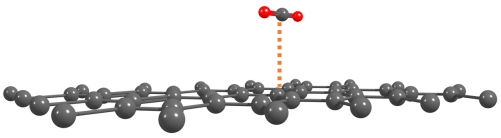

Figure 3.8: Monolayer of graphene and CO_2 without any interactions.

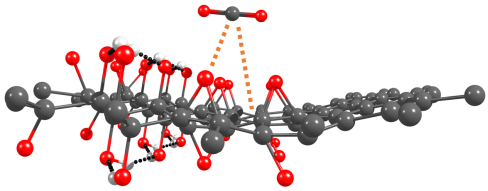

Figure 3.9: Monolayer of graphene oxide adsorbing a CO_2 molecule.

3.4 Hydrogel synthesis

PAM-based hydrogels are commonly prepared through a free radical polymerization method, in which acrylamide monomers react through a cross-linking effect to form long chains of polyacrylamide. The degree of cross-linking can be controlled or adjusted by operating at the temperature, type of cross-linker, initiator, or catalyst [41].

This study focuses on different PAM-based hydrogels that were synthesized through a redox-initiated radical polymerization system, whose initiation process features:

- Potassium Persulfate (KPS): Which acts as an oxidizing agent during its decomposition, generating sulfate radicals (SO_4^-). It is a common radical polymerization primary initiator, able to start the polymerization at room temperature in the presence of TMEDA;
- Tetramethylethylenediamine (TMEDA): It is a Lewis base that acts as a co-initiator by serving as the reducing agent, accelerating the decomposition of KPS into radicals and enhancing the radical initiation efficiency. Specifically, it donates an electron to persulfate, generating sulfate radicals.

KPS acts on the acrylamide monomers, turning them into free radicals, which bind together by covalent forces with the monomers that are not activated to start the chain reaction of polymerization until a gel is generated.

The combined utilization of KPS and TMEDA allows effective control of the gelation [3] process, fast polymerization at room temperature conditions, and flexibility in the reactions, permitting the formation of a chemically cross-linked hydrogel network.

[3]It stands for gel transition, regarding the formation of a gel from a system with polymers.

The concentration of the radical initiators can also affect the polymerization process as well as the properties of the hydrogels [41]:

- High concentration: More but shorter polymer chains, inelastic gels, high turbidity;
- Low concentration: Fewer but longer polymer chains, elastic gels, low rate of polymerization, and high porosity.

The purpose of this work study is the synthesis and characterization of six different types of hydrogels, whose composition is summarized in the table 3.4. Each of them was constructed in ambient conditions and tested its CO_2 adsorption capabilities inside an airtight container under similar conditions for 24 hours. After that, the best-performing gels were doped by adding amino groups, aiming at increasing the gel reactivity and selectivity towards CO_2, enhancing the performance from their plain version.

Hydrogel	Water	KPS	TMEDA	AM	CA	GO	GO-COOH
Plain	63%	0.15%	0.2%	36.6%	/	/	/
Plain/CA	63%			18.3%	18.3%	/	/
GO	31.5%			36.6%	/	31.5%	/
GO/CA	31.5%			18.3%	18.3%	31.5%	/
GO-COOH	31.5%			36.6%	/	/	31.5%
GO-COOH/CA	31.5%			18.3%	18.3%	/	31.5%

Table 3.4: Employed hydrogels overview.

All hydrogels, despite having different compositions, were synthesized to have a standardized weight (15,85 g) to facilitate the analysis, while allowing a fair comparison between them. AM and CA stand for Acrylamide and Citric Acid respectively. Each compound concentration is expressed as a weight percentage (wt%), which indicates the mass of every substance relative to the total mass of the mixture, multiplied by 100.

The modification of plain Polyacrylamide (PAM)-based hydrogels by reducing the quantity of Acrylamide and replacing it with Citric acid may tune some specific properties, such as elasticity and porosity, as well as introducing additional carboxyl groups within the matrix, potentially enhancing hydrophilicity and generating a more diverse network.

3.5 Characterization tests

A comprehensive understanding of the aspects of the synthesized hydrogels can be evaluated with the help of various characterization tests:

- Fourier Transform Infrared Spectroscopy (FTIR): Executed with an IRXross FTIR Spectrophotometer, it is an analytical technique that utilizes infrared light to analyze the chemical properties of the gels, identifying the functional groups. A multi-frequency beam of light is shined to measure how much of that is absorbed by the sample. The beam is then modified to have a different combination of frequencies, giving out a second data point. This process is quickly repeated multiple times over a short period. At last, a computer takes care of all the data and works backward to infer what the absorption is at each wavelength.

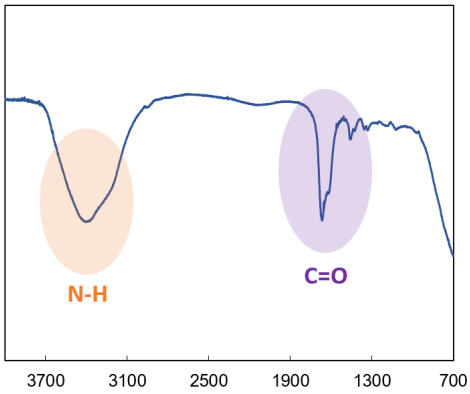

Figure 3.10: GO hydrogel FTIR, displayed as transmittance [a.u.] v. wavenumber $[cm^{-1}]$.

- Raman spectroscopy: Chemical analysis able to investigate a substance's chemical structure and molecular interactions. It relies upon the inelastic scattering of photons. A source of monochromatic light, usually from a laser operating in the visible, either near-infrared or near-ultraviolet range, interacts with molecular vibrations and other excitations in the system, resulting in the energy of the laser photons being shifted up or down. The energy shift quantifies the vibrational modes in the system. It is expressed as the intensity [a.u.] v. Raman shift $[cm^{-1}]$;

- Differential Scanning Calorimetry (DSC): Useful method to examine the thermal transitions that take place in a material whenever it gets heated up. The energy required to heat a sample is then compared to the one of a reference material [42].

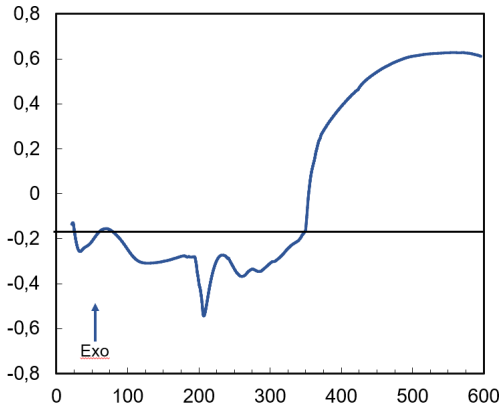

Figure 3.11: GO hydrogel DSC, displayed as heat flow [W/kg] v. temperature [°C].

- Thermo-Gravimetric Analysis (TGA): Carried out with a TA Instruments SDT650 analyzer, it is an experimental method that focuses on the thermal stability of a material by comparing how its physical properties, expressed as a mass loss, change to a certain heat rate. The final mass is then compared to the initial one to quantify the actual diminution.

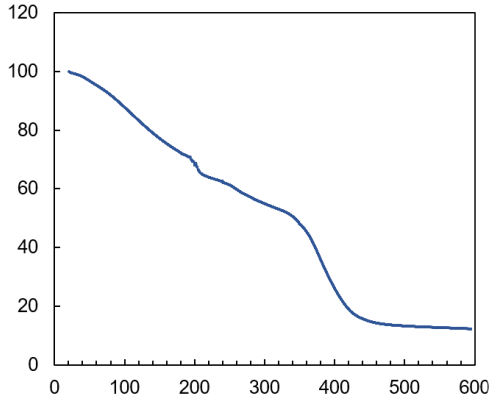

Figure 3.12: GO hydrogel TGA, displayed as weight loss [%] v. temperature [°C].

- X-ray diffraction analysis (XRD): Non-destructive analytical strategy executed to scatter X-rays over the atomic structure of a crystalline material, allowing

to provide details about its structure. More precisely, the intensities and the angles of the X-rays are taken into account to determine a unique diffraction pattern for every material. It is expressed as the intensity [a.u.] v. angle of diffraction [2θ].

3.6 Experimental methods

3.6.1 Sensor setup

All experimental data was gathered using an E+E EE892 CO_2 sensor [43], which is considered to be a reliable instrument to evaluate carbon dioxide fluctuations over a long period inside a controlled environment. The sensor specifically features:

- Non-Dispersive Infrared (NDIR) technology: It detects carbon dioxide based on its absorption of infrared light;
- Original Equipment Manufacturers (OEM) applications: Meaning that it can integrated to large-scale devices, such as HVAC systems or air quality tracking.

The measurement range is up to 10000 ppm, with an accuracy of $\pm$100 ppm, as the device is connected to an Arduino Uno micro-controller board [44] for data collection and analysis, as visible in the figure 3.13.

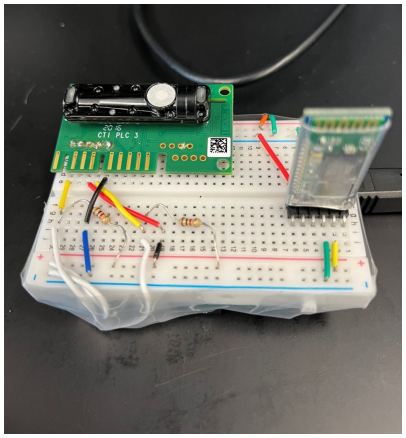

Figure 3.13: EE892 sensor linked to Arduino through a breadboard, allowing to connect and disconnect components without welding.

More precisely, the employed electrical device displays the following quantities:

1. Temperature [°C];
2. Relative humidity (RH) [%];

3. Mean CO_2 level [ppm] over the selected time range;

4. Pressure [mbar].

3.6.2 Vessel fabrication and leakage test

Graphene oxide-based hydrogels need to be experimentally tested inside an airtight vessel, that allows the generation of a leak-free controlled environment, which is ideal for achieving consistency in testing.

Polycarbonate was selected to be the optimal vessel material for this case study since it appears to be a resistant thermoplastic polymer, able to offer both UV and thermal resistance, and is very easy to work with. Additionally, it is lightweight and transparent, permitting to always visualize the hydrogel during each 24-hour test.

Large polycarbonate blocks were divided into small rectangular sheets by utilizing a laser cutter machine, which vaporizes materials through high-power laser beams. After that, the single sheets were glued together by applying the solvent-cement Weldon #4, which is a clear fast-setting adhesive that works by melting plastic surfaces together. Lastly, an epoxy-based resin was added to provide additional sealing at the cube edges.

Various 24-hour leakage tests were performed by just inserting the sensor with no hydrogel to ensure the assembled container was leak-free. Experimental tests were instead carried out by inserting each hydrogel from the table 3.4 over a 3D-printed ABS [4] holder.

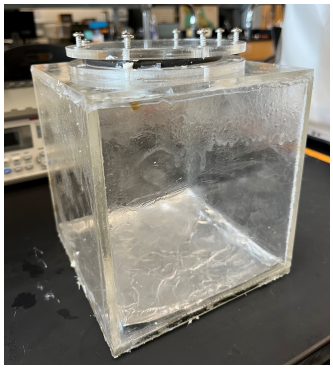

Figure 3.14: Airtight container side view.

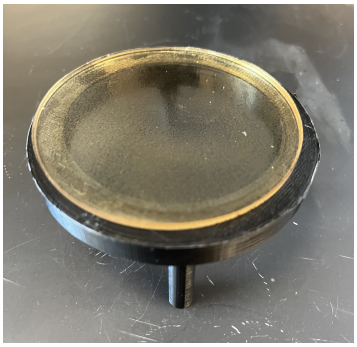

Figure 3.15: 3D printed hydrogel holder.

[4]Standing for Acrylonitrile Butadiene Styrene, it is a common recyclable polymer employed for 3D printings because of its strength and durability.

Chapter 4

Results

4.1 Polyacrylamide hydrogels

All PAM hydrogels illustrated in the table 3.4 were tested at equal conditions inside the polycarbonate airtight vessel for 24 hours. Carbon dioxide was injected inside the sealed environment by using a compressed CO_2 cylinder, which allows a continuous flow of the gas until the desired concentration is obtained. All hydrogels were compared depending on their adsorption performance starting with a 6500 ppm environment, at ambient temperature and pressure.

The observed results after a period of 24 hours are shown in the figures 4.1, 4.2.

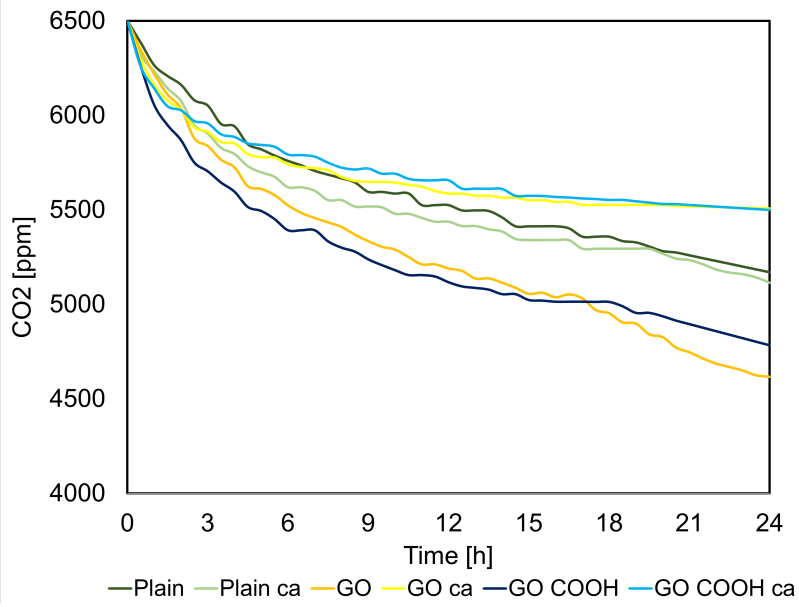

Figure 4.1: Absolute CO_2 variation over time referred to every PAM hydrogel.

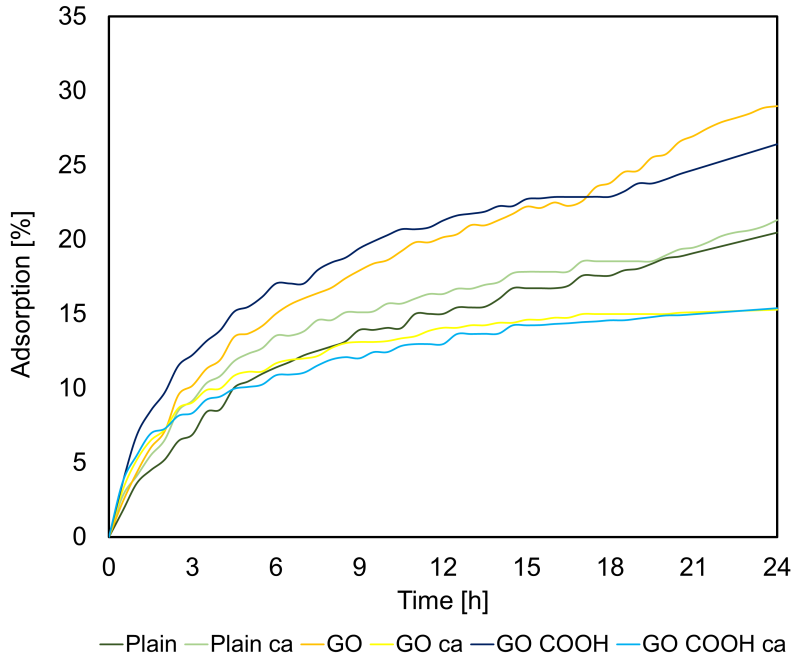

Figure 4.2: CO_2 percentage uptake comparison.

The performances can also be compared under the following two entities, as also expressed in the table 4.1:

- Adsorption capacity [mmol/g]:

$$Capacity_{ads} = \frac{Moles_{CO_2}}{Mass_{gel}} = \frac{Uptake_{abs} \cdot V_{vessel}}{1000 \cdot V_{molar} \cdot m_{gel}} \tag{4.1}$$

- CO_2 capture efficiency [%]:

$$\eta_{capture} = \frac{(CO_{2initial} - CO_{2final})}{CO_{2initial}} \cdot 100 \tag{4.2}$$

Parts per million of CO_2 are converted using the Ideal gas law, where:

- Molar volume = V_{molar} = 22,414 L/mol
- Airtight vessel volume = V_{vessel} = 3,123 L
- Gel mass = m_{gel} = 15,85 g

Hydrogel	Absolute uptake [ppm]	Adsorption capacity [mmol/g]	Capture efficiency [%]
Plain	1330	0,012	20
Plain/CA	1385	0,012	21
GO	1883	0,017	29
GO/CA	993	0,009	15
GO-COOH	1717	0,015	26
GO-COOH/CA	1000	0,009	15

Table 4.1: PAM hydrogels measured performance overview.

The outcomes reveal that hydrogels modified with GO and GO-COOH exhibit significantly enhanced CO_2 adsorption capacities compared to their plain counterparts. Capture efficiencies of 31% and 26% respectively indicate that these modifications have definitely enhanced their performance.

In contrast, plain hydrogels demonstrate the lowest adsorption rates, showing the limited effectiveness of unmodified mixtures. The decision to add citric acid was based on the hypothesis that both swelling and adsorption capacity would have been boosted. However, a worse performance highlights that hypothesis's limitations, guiding different future modifications.

The data also suggest that a notable portion of the absolute CO_2 adsorption derives from the first 5 hours of testing, as 51% for plain gels, 44% for GO-based, and 58% for GO-COOH-based ones.

4.2 Functionalization with amines

As both GO and GO-COOH-based hydrogels were selected as the best-performing ones, a further modification was carried out by doping them with three different Amines, as represented in the table 4.2. Amino groups generally have several impacts on the hydrogel performance, such as:

- Enhanced CO_2 adsorption capability: The chemical interaction amine-carbon dioxide is stronger than the one occurring with plain gels;
- Better selectivity for CO_2 over other atmospherical gases, like N_2;
- Self-healing properties due to the formation of new reversible bonds;
- Upgraded interaction with moisture, making doped-hydrogels ideal for humid environments.

The added amines quantity certainly makes the difference, as wrong ratios can result in the gel turning too slimy and sticky and hard to work with. Overall, in

order to maintain good reactivity and properties, the quantity was determined to be 40 μL, added to the mixture through small drops while stirring, leading to a rigid final consistency.

Amino group name	Structure	wt%
Ethylenediamine	$NH_2 - CH_2 - CH_2 - NH_2$	0,25% (40μL)
Bis(3-aminopropyl)amine	$NH_2 - (CH_2)_3 - NH - (CH_2)_3 - NH_2$	0,25% (40μL)
Urea	$O = C(NH_2)_2$	0,25% (39,5mg)

Table 4.2: Employed amino groups with respective quantities.

The CO_2 trend results gathered after testing the improved versions of both GO and GO-COOH hydrogels from 6500 ppm for 24 hours are displayed in the figures 4.3, 4.4. The following table 4.3 represents the adsorption capacities and efficiencies, respectively estimated with the same criteria as with the plain versions of the gels, allowing a fair correlation between all versions.

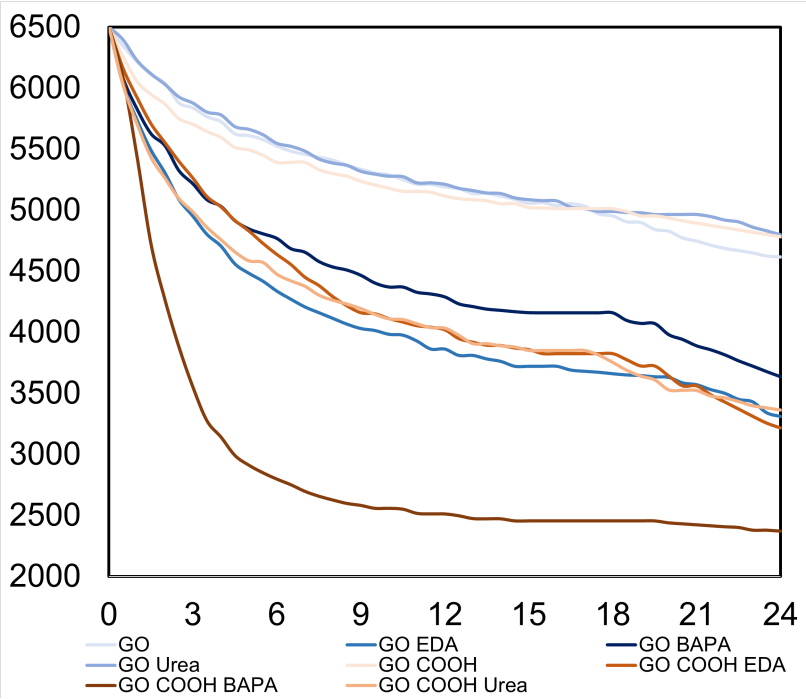

Figure 4.3: Absolute CO_2 variation over time referred to every amino-doped hydrogel.

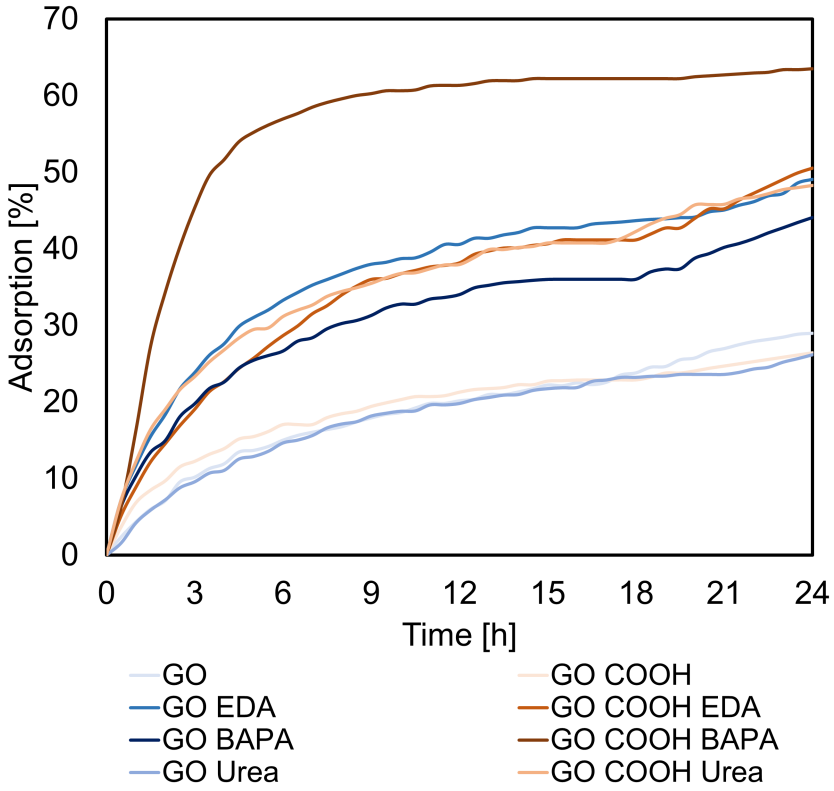

Figure 4.4: CO_2 percentage uptake comparison.

Hydrogel	Absolute uptake [ppm]	Adsorption capacity [mmol/g]	Capture efficiency [%]	CO_2 loading
GO	1883	0,017	29	/
GO/EDA	3189	0,028	49	0,33
GO/BAPA	2865	0,025	44	0,88
GO/Urea	1702	0,015	26	0,18
GO-COOH	1717	0,015	26	/
GO-COOH/EDA	3284	0,029	51	0,35
GO-COOH/BAPA	4129	0,036	64	1,26
GO-COOH/Urea	3137	0,028	48	0,33

Table 4.3: Amino-doped hydrogels measured performance overview.

In accordance with the expectations, the amino-modified hydrogels showed enhanced carbon capture uptake, except for the case of GO with urea. The carboxylated graphene oxide versions have shown the most significant performance upgrade with respect to the plain versions, whereas the GO hydrogels have improved less. Specifically, the GO-COOH BAPA hydrogel demonstrated the highest adsorption capacity and capture efficiency values, reaching 64% CO_2 uptake and providing the fastest kinetics. The other GO-COOH hydrogels performed similarly, with adsorption capacities of 48% and 51% respectively.

The table 4.3 also compares the hydrogels based on their CO_2 loading, which is a common element to characterize amino-functionalized species, referring to:

$$CO_{2loading} = \frac{Moles_{CO_2}}{Moles_{Amine}} \tag{4.3}$$

It is found to be useful as it allows the selection of modified materials based on the gas capture per functional group.

All three employed amines contain two primary amino groups, as described in the table 4.2. In particular, the GO COOH BAPA gel showcases a CO_2 loading higher than 1, as it also contains a secondary amino group that exhibits high reactivity towards carbon dioxide. This results in a molecule of BAPA having multiple adsorption sites, leading to strong chemisorption interactions and a large capacity with respect to its counterparts.

It is also evident that most of the adsorption comes in the first hours of testing, as well as in the case of plain GO and GO COOH gels. For instance, by observing the GO COOH BAPA CO_2 trend in figure 4.3, it can be estimated that 85% of the total capture comes just in the first 5 hours. This phenomenon mainly occurs because the initial concentration gradient between the gas phase and the adsorbent is the largest, increasing the diffusion driving force. Moreover, amines facilitate rapid carbon dioxide chemisorption, which leads to an early saturation of the active sites. After a quick diffusion through the gel pores, most sites turn occupied, leading to limited availability and consequent pore-blocking effects, while slowing down the adsorption rate. Eventually, the closed system reaches the state of equilibrium, where the rate of adsorption equals the one of desorption.

Overall, the data proved that incorporating GO and GO-COOH with amines can considerably increase the gels' effectiveness, substantially doubling the performance of the plain versions.

Adsorption is generally a dynamic process comprising multiple variable factors over time, such as temperature, pressure, and relative humidity. These parameters were examined based on the sensor outputs and displayed in figure 4.5, as they provide a precise description of the interactions occurring inside the airtight container.

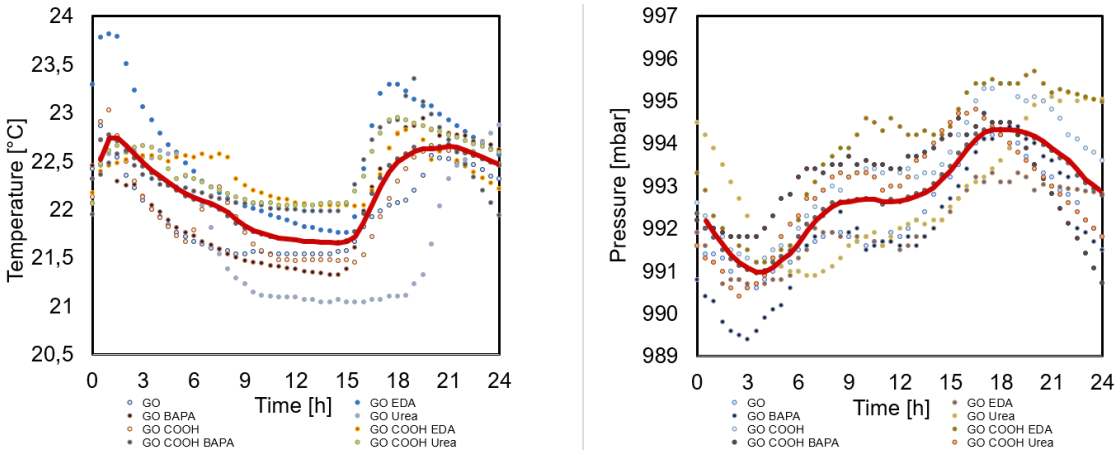

Figure 4.5: Temperature and pressure trends over time, with respective trendlines.

In the first hours of testing, early adsorption reduces the quantity of CO_2 molecules in the air, bringing down the partial pressure of the gas inside the vessel. In the meantime, the intrinsic exothermic nature of the process produces heat, resulting in an initial temperature rise. These mechanisms occur simultaneously but are actually independent of each other as a matter of driving forces.

Later on, as the employed hydrogels approach the saturation of their available sites, the heat generation released by CO_2 binding decreases, resulting in a cooling effect. Insufficient adsorption associated with a small release of gas back into the gas phase can cause the pressure to increase, justifying the observed upward trend.

Between the 9th and the 15th hour of testing, the system appears to reach thermodynamic equilibrium, as adsorption and desorption rates turn equivalent, guiding temperature and pressure to stabilize.

In the interval of the 15th and the 18th hour, the synchronous growth of the two thermodynamic variables could be due to a slight desorption of CO_2, which increases the partial pressure of the system and generates heat, or some structural changes in the material, whose relaxation phase is exothermic. According to the ideal gas law, a temperature-pressure coupling could also be induced, as an increment in the kinetic energy of particles may increase pressure too.

At the adsorption rate reaches its limit at the end of testing, a minor cooling effect could result in a slight temperature and pressure drop as stabilization is obtained, so that both quantities settle to their initial values. The polycarbonate material, as well as the sealants, constituting the vessel insulation properties, could also play a role by driving the system variables to evolve in complex ways.

4.3 Experimental limitations

The captured carbon dioxide may be recovered by regenerating the sorbents through endothermic desorption processes, thus supplying energy. They can be carried in three ways:

- Temperature Swing Adsorption (TSA): Promising and effective, it is employed by heating up the solid adsorbent to break the chemical bonds, releasing the captured gas. Conventional bulk heating at 120°C results in being very energy-intensive, therefore microwave irradiation methods are gaining success as they occur at low temperatures (50°C). In particular, waveguide microwave applicators testing ensures 90% desorption in around 10 minutes [45]. However, most of the incident microwave power does not contribute to CO_2 desorption due to impedance mismatching, causing a high reflection rate and low efficiency;
- Pressure Swing Adsorption (PSA): By depressurizing the system, pushing the material to release the adsorbed gas. Mostly employed in hydrogen purification and air separation fields;
- Vacuum Swing Adsorption (VSA): Pressure is reduced by utilizing a vacuum pump, leading the adsorbed gas to leave the surface more easily. It is found to be effective for low-pressure gas capture in DAC purposes.

Desorption time is often dictated by the heat transfer rate, which is the main CO_2 productivity limiting driver. An option to overcome both sorbent stability and heat transfer limitations is the usage of electric energy, through microwave and induction-based methods, since dielectric heating results in being better-performing than the conventional thermal one. However, further research is necessary on the feasibility of large-scale applications as well as the impacts on material stability.

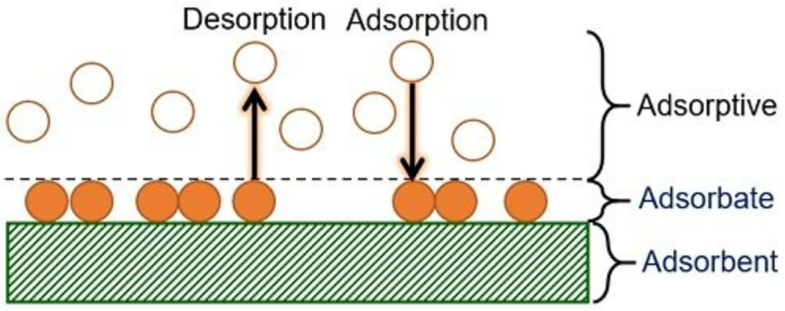

Figure 4.6: Visual representation of the main factors acting during the process.

Regeneration energy is related to both the heat capacity and the reaction enthalpy of CO_2 binding. It still remains challenging today, as developing sorbents that can be regenerated using the same or less amount of energy released during the flue gas capture process represents an ideal energy-neutral scenario for making a capture technology appealing to the market.

The carbon dioxide capture performance of the employed hydrogels is dependent on several factors and can be further improved by increasing the specific surface area (SSA) and tuning the CO_2 concentration inside the enclosed container environment, providing extra adsorption active sites. From the literature, the adsorption capacity of solid adsorbents should be in the order of 3 mmol/g to develop a sustainable large-scale capture technology [46] [47]. Such a threshold might be reached with superior engineered materials that exhibit high SSAs, such as Conjugated Microporous Polymers (CMPs) with 600 m^2/g, Hyper-Crosslinked Polymers (HCPs) with 2000 m^2/g [47], and Metal-Organic Frameworks (MOFs) with up to 10000 m^2/g, [48]. Moreover, most of the experimental tests are carried out using dry steams of 10% to 100% CO_2, as the observed adoption capacity is directly proportional to the partial pressure of carbon dioxide, and higher concentrations generate stronger driving forces.

This work is limited to experimental testing under 6500 ppm ambient (0,65% CO_2) as a constraint imposed by the employed EE892 sensor, allowing an acceptable level of accuracy in the measurement. As the hydrogels were synthesized inside 9 cm circular plates, with a mass calculated to be 15,85 g, the overall SSA can be estimated as 4 cm^2/g, well far from the high-performance nanoporous materials of the literature.

Both the hydrogels' mass and surface area, and consequently the adsorption capacity, can be enhanced by reducing the water content in the preparation, optimizing the ratios of the utilized components, such as the loading of GO and GO COOH, and increasing the number of micropores ($<$ 2nm) and mesopores (2-50 nm). This may be achieved by utilizing pore-forming agents and by freeze-drying the gel, which is a low-temperature dehydration process, allowing the removal of the solvent, thus generating high internal porosity, as in the case of Aerogels.

An additional way to emphasize different types of hydrogel other than their adsorption capacities is by analyzing the mechanical properties that can be achieved by a variety of chemical configurations. Principal qualities of interest such as tensile and compressive strength, Young's modulus, stiffness, creep, fatigue behavior, and swelling ratios [1] are a complement to adsorption tests as they result in being essential in the characterization carried out by this work.

[1]Also known as the degree of swelling, indicated as a percentage, it quantifies the ability of a material to absorb fluid and expand in size. It is dependent on the solvent nature, network density, and interaction polymer-solvent.

PAM-based hydrogels with a high swelling ratio feature a diluted network, resulting in low tensile strength (MPa) and high elongation at break (%), and vice-versa. The amount of crosslinker also plays a crucial role, as large values of it determine a high degree of swelling and low tensile strength [49].

Tensile testing by pulling on both ends of hydrogels can also generate a small electric voltage, following a phenomenon known as the piezoelectric effect, occurring with materials able to create an electric charge in response to applied mechanical stress. Of course, whether a specific hydrogel will produce voltage during a tensile test depends on its composition and properties. For this case study, acrylamide, TMEDA, and KPS do not possess inherent piezoelectric properties, but the hydrogel exhibits the effects as a consequence of its design. Specifically, when GO gets incorporated into the hydrogel, it may develop a hybrid structure that has some unique properties due to its ability to polarize under mechanical deformation. Also, KPS and TMEDA are responsible for a network structure where an applied mechanical force can induce charge redistribution, facilitating ion and electron movement following a deformation. Nanomaterials like graphene oxide might also lead to a mechanical-electrical feature coupling, converting one to the other once the material is applied to a load.

Overall, it is key to take into account the environment in which the materials will be used once the mechanical properties are identified, in order to guarantee a proper assessment of the study.

Chapter 5

Conclusion and Future Outlook

The proposed PAM hydrogels have demonstrated a notable potential as an effective adsorbent for CO_2 capture applications in this work-study. It was noticed that the specific adsorbance was substantially boosted with the addition of graphene oxide (GO), which features a specific surface area of 2418 m^2/g [50], offering the gel a porous structure with more active sites, increasing both the interaction with the gas and the adsorption capacity, as demonstrated via experimental tests.

An investigation was therefore carried out by functionalizing both GO and GO COOH gels with three types of amines, which appeared to significantly enhance the performance in terms of adsorption capacity, and efficiency. Adsorption tests specifically highlighted Ethylenediamine (EDA) and Bis3(Aminopropyl)amine (BAPA) as the most effective modifications. Amino groups (NH_2) are capable of creating strong interactions with carbon dioxide, forming carbamates and bicarbonates. Overall, the kinetics of the reaction and selectivity towards the gas phase are found to be upgraded. Amines can then be regenerated in multiple ways after binding with CO_2 molecules through heating or specific conditions, making it ideal for industrial capture purposes, as the entire process becomes cyclic and sustainable.

Future work would focus on and be dedicated to the SSA improvement, which would guarantee a higher absorption capacity in terms of mmol/g, a detailed characterization of the proposed hydrogels' mechanical features, and the realization of efficient ways to desorb the adsorbed CO_2, allowing the regeneration of the employed materials.

Possible applications of GO-doped hydrogels may include the realization of small passive filtering systems able to improve indoor air quality inside work offices, public transportation systems, and commercial aircraft.

It has been demonstrated that high carbon dioxide levels (>1000 ppm) in indoor ambient are strongly linked to reduced work performance, an increased likelihood of health issues, and poorer perceived air quality [51]. Keeping both CO_2 and volatile organic compounds (VOCs) concentrations under a certain limit also limits the propagation of bacteria and viruses. The proposed hydrogels may also be introduced in specific polluted open-air environments typical of large cities, such as busy intersections or roundabouts, where pedestrians can be easily found.

Bibliography

[1] National Oceanic and Atmospheric Administration. *Trends in CO_2, CH_4, N_2O, SF_6*. 2024. URL: https://gml.noaa.gov/ccgg/trends/ (cit. on p. 1).

[2] I%EC research. *The Role of Carbon Capture and Utilization, Carbon Capture and storage, and Biomass to Enable a Net-Zero-CO2 Emissions chemical industry*. 2020. URL: https://pubs.acs.org/doi/epdf/10.1021/acs.iecr.9b06579?ref=article_openPDF (cit. on p. 1).

[3] IPCC. *Sixth Assessment Report*. 2023. URL: https://www.ipcc.ch/assessment-report/ar6/ (cit. on pp. 2, 5).

[4] IPCC. *Sixth Assessment Report, Chapter 7*. 2023. URL: https://www.ipcc.ch/report/ar6/wg1/chapter/chapter-7/ (cit. on p. 2).

[5] IPCC. *The current state of the climate*. 2020. URL: https://www.ipcc.ch/report/ar6/wg1/chapter/summary-for-policymakers/ (cit. on p. 3).

[6] Zurich Insurance Group. *Climate refugees*. 2024. URL: https://www.zurich.com/media/magazine/2022/there-could-be-1-2-billion-climate-refugees-by-2050-here-s-what-you-need-to-know (cit. on p. 6).

[7] IEA. *CO_2 emissions by sector*. 2022. URL: https://www.iea.org/data-and-statistics/data-tools/energy-statistics-data-browser?country=WORLD&fuel=CO2%20emissions&indicator=CO2BySector (cit. on p. 8).

[8] Our world in data. *Emissions by sectors*. 2022. URL: https://ourworldindata.org/ghg-emissions-by-sector (cit. on p. 8).

[9] European Commission. *EU ETS emissions cap*. 2022. URL: https://climate.ec.europa.eu/eu-action/eu-emissions-trading-system-eu-ets/eu-ets-emissions-cap_en (cit. on p. 9).

[10] IEA. *Sustainable Development Scenario relative to the Stated Policies Scenario*. 2020. URL: https://www.iea.org/data-and-statistics/charts/global-co2-emissions-reductions-in-heavy-industry-by-mitigation-strategy-in-the-sustainable-development-scenario-relative-to-the-stated-policies-scenario-2070 (cit. on p. 9).

[11] Francesco Miccio Federica Raganati and Paola Ammendola. «Adsorption of Carbon Dioxide for Post-combustion Capture: A Review». In: *Energy % Fuels* 35 (Oct. 2021), pp. 12845–12868 (cit. on p. 11).

[12] Mercedes Moroto-Valer Dennis Y C Leung G. Caramanna. «An Overview of Current Status of Carbon Dioxide Capture and Storage Technologies». In: *Renewable and Sustainable Energy Reviews* 1 (Nov. 2014), pp. 429–431 (cit. on p. 12).

[13] Rujing Hou, Celesta Fong, Benny D Freeman, Matthew R. Hill, and Zongli Xie. «Current status and advances in membrane technology for carbon capture». In: *Separation and Purification Technology* 1 (Nov. 2022), p. 3 (cit. on p. 12).

[14] IEA. *Is carbon capture too expensive?* 2021. URL: `https://www.iea.org/commentaries/is-carbon-capture-too-expensive` (cit. on pp. 12, 13).

[15] Laura Gagliardi Jenny G Vitillo Berend Smit. «Introduction: Carbon Capture and Separation». In: *Chemical Reviews* 1 (July 2017), p. 9521 (cit. on p. 12).

[16] Dowell Mai Bui Niall Mac. *Carbon capture and storage (CCS): the way forward*. 2018. URL: `https://pubs.rsc.org/en/content/articlelanding/2018/ee/c7ee02342a` (cit. on p. 14).

[17] Global CCS Institute. *Technology Readiness and Costs of CCS*. 2021. URL: `https://www.globalccsinstitute.com/resources/publications-reports-research/technology-readiness-and-costs-of-ccs/` (cit. on p. 14).

[18] Yarasi Soujanya. «CO2 adsorption by functionalized sorbents.» In: *Polymer and Functional Materials* 192 (Aug. 2020), pp. 229–240 (cit. on pp. 15, 16).

[19] B. Adderley, J. Gibbins J. Carey, and R. Smith M. Lucquiaud. «Post-combustion carbon dioxide capture cost reduction to 2030 and beyond.» In: *Faraday Discuss* 192 (July 2016), pp. 27–35 (cit. on p. 15).

[20] Alka Tangri. «Polyacrylamide based hydrogels: synthesis, characterization and applications.» In: *IJPCBS* 4 (Apr. 2014), p. 951 (cit. on pp. 17, 18).

[21] Enas M. Ahmed. «Hydrogel: Preparation, characterization, and applications: A review.» In: *Cairo University: Journal of Advanced Research* 1 (July 2013), p. 107 (cit. on pp. 17, 18).

[22] Nazar Muhammad Ranjha Muhammad Faheem Akhtar Muhammad Hanif. «Methods of synthesis of hydrogels ... A review». In: *Saudi Pharmaceutical Journal* 24 (Sept. 2016), pp. 554–559 (cit. on p. 17).

[23] Illeperuma W Sun JY Zhao X. «Highly stretchable and tough hydrogels.» In: *Nature* 489 (Sept. 2012), pp. 133–136 (cit. on p. 18).

[24] Wang M. X. Yang C. H., Yang J. H. Haider H., Chen Y. M. Sun J.-Y., and J. Zhou. «Strengthening Alginate/Polyacrylamide Hydrogels Using Various Multivalent Cations.» In: *ACS Applied Materials & Interfaces* 5 (Sept. 2013), pp. 10418–10423 (cit. on p. 18).

[25] An Zhao Arunkumar Samanta, Partha Sarkar George K. H. Shimizu, and Rajender Gupta. «Post-Combustion CO2 Capture Using Solid Sorbents: A Review.» In: *Industrial & Engineering Chemistry Research* 51 (Oct. 2011), pp. 1438–1463 (cit. on p. 18).

[26] Asbury Carbons. *Natural Flake Graphite*. 2024. URL: `https://www.asbury.com/materials/graphite/` (cit. on p. 19).

[27] Ilhan A. Aksay Michael J. McAllister. «Single Sheet Functionalized Graphene by Oxidation and Thermal Expansion of Graphite.» In: *Princeton Institute for the Science and Technology of Materials* 1 (Feb. 2007), p. 1 (cit. on p. 20).

[28] Stankovich S., Dommett G. H. B. Dikin D. A., Zimney E. J. Kohlhaas K. M., and Stach E. A. «Graphene-based composite materials». In: *Nature* 442 (Feb. 2006), pp. 282–286 (cit. on p. 20).

[29] Stankovic B., Sanz O. Barbarin I., and Ruiperez Tomovska R. «Experimental and theoretical study of the effect of different functionalities of graphene oxide/polymer composites on selective CO_2 capture.» In: *Scientific Reports* 12 (Mar. 2022), p. 15992 (cit. on p. 20).

[30] Graphenea. *Graphene - What Is It?* 2024. URL: `https://www.graphenea.com/pages/graphene-oxide` (cit. on p. 20).

[31] Cristina Gomez-Navarro, Ravi S. Sundaram Jannik C. Meyer, Simon Kurasch Andrey Chuvilin, Klaus Kern Marko Burghard, and Ute Kaiser. «Atomic Structure of Reduced Graphene Oxide». In: *NANO-Letters* 4 (Mar. 2010), pp. 1144–1148 (cit. on p. 20).

[32] Chun Li Ji Chen Bowen Yao and Gaoquan Shi. «An improved Hummers method for eco-friendly synthesis of graphene oxide». In: *Carbon* 64 (Nov. 2013), pp. 225–229 (cit. on p. 21).

[33] Liu Yanan Jingzhong Liu Chen Shuping and Zhao Bijing. «Progress in preparation, characterization, surface functional modification of graphene oxide: A review». In: *Journal of Saudi Chemical Society* 26 (Nov. 2022), p. 101560 (cit. on p. 21).

[34] Richard E. Offeman William S. Hummers Jr. «Preparation of Graphitic Oxide». In: *Journal of the American Chemical Society* 80 (Mar. 1958), p. 6 (cit. on p. 21).

[35] Yuan Li, Laurent Galmiche Valérie Alain-Rizzo, Fabien Miomandre Audebert Pierre, Michael Bozlar Guy Louarn, and Michael A. Pope. «Functionalization of Graphene Oxide by Tetrazine Derivatives: A Versatile Approach toward Covalent Bridges between Graphene Sheets». In: *Chemistry of Materials* 27 (May 2015), p. 12 (cit. on p. 22).

[36] Carbon composites (Second edition). *Sonication*. 2017. URL: https://www.sciencedirect.com/topics/engineering/sonication#:~:text=Sonication%20is%20a%20process%20of,the%20solution%20containing%20the%20liposomes. (cit. on p. 23).

[37] Saddam Hossain, Loknath Dhar Md Sajjadur Rahman, Quraishi Shamshad B., Farzana Rahman Md Nurul Abser, and Mir Tamzid Rahman. «Increasing the potentiality of graphene oxide by chloroacetic acid for the adsorption of lead with molecular dynamic interpretation». In: *Current Research in Green and Sustainable Chemistry* 4 (May 2021), p. 100095 (cit. on p. 24).

[38] Gayanath W. Fernando. «Metallic Multilayers and their Applications». In: *Handbook of Metal Physics* 4 (May 2008), p. 220 (cit. on p. 25).

[39] Giannozzi P. «QUANTUM ESPRESSO: a modular and open-source software project for quantum simulations of materials». In: *Handbook of Metal Physics* 21 (Sept. 2009), p. 395502 (cit. on p. 25).

[40] M. I. Katsnelson D. W. Boukhvalov. «Chemical Functionalization of Graphene with Defects». In: *ACS publications* 1 (Oct. 2008), p. 130 (cit. on p. 25).

[41] Gangadevi Sennakesavan, L.K. Dkhar Mohammad Mostakhdemin, and S.J. Fatihhi Ali Seyfoddin. «Acrylic acid/acrylamide based hydrogels and its properties - A review». In: *Polymer Degradation and Stability* 180 (Oct. 2020), p. 109308 (cit. on pp. 26, 27).

[42] E. Smith R. Harwood. «Testing of natural textile fibres». In: *Handbook of Natural Fibres (Second Edition)* 180 (Sept. 2020), pp. 535–576 (cit. on p. 29).

[43] Epluse. *EE892 sensor*. 2024. URL: https://www.google.com/url?sa=i&url=https%3A%2F%2Fwww.epluse.com%2Ffileadmin%2Fdata%2Fproduct%2Fee892%2Fdatasheet_EE892.pdf&psig=AOvVaw3yxGb5QfmOOj-5NTMmC6s3&ust=1730890032798000&source=images&cd=vfe&opi=89978449&ved=0CAQQn5wMahcKEwjggLH9hMWJAxUAAAAAHQAAAAAQBA (cit. on p. 30).

[44] Arduino. *Arduino Uno Rev3 board*. 2024. URL: https://store.arduino.cc/products/arduino-uno-rev3?gad_source=1&gclid=Cj0KCQiAoae5BhCNARIsADVLzZfFePawEaHMBZoUgy7qJjb39-cSsSRyZ0VzKlM__j8gcPiK4gOh3QkaAsHNEALw_wcB (cit. on p. 30).

[45] Brian R Ellis Tae Hwan Lim John E Foster and Steven J Skerlos. «Microwave-based CO2 desorption for enhanced direct air capture: experimental validation and techno-economic perspectives». In: *Environmental research* 19 (Feb. 2024), p. 34002 (cit. on p. 39).

[46] Ziyi Zhong Qiang Wang Jizhong Luo and Armando Borgna. «CO2 capture by solid adsorbents and their applications: current status and new trends». In: *Energy & Environmental science* 1 (Dec. 2010), p. 12 (cit. on p. 40).

[47] Ziyi Zhong Junya Wang. «Recent advances in solid sorbents for CO2 capture and new development trends». In: *Energy & Environmental science* 1 (Aug. 2014), p. 13 (cit. on p. 40).

[48] Shashank Sundriyal Vaishali Shrivastav. «Recent advances on surface mounted metal-organic frameworks for energy storage and conversion applications: Trends, challenges, and opportunities». In: *Advances in Colloid and Interface Science* 318 (Aug. 2023), p. 102967 (cit. on p. 40).

[49] Mark Ahearne. «Mechanical testing of hydrogels». In: *The Mechanics of Hydrogels* 1 (Aug. 2022), pp. 73–90 (cit. on p. 41).

[50] Jianping Liu Songdi Zhang Huihui Wang and Chenlu Bao. «Measuring the specific surface area of monolayer graphene oxide in water». In: *Materials Letters* 261 (Feb. 2020), p. 127098 (cit. on p. 42).

[51] William J Fisk Usha Satish. «Is CO2 an Indoor Pollutant? Direct Effects of Low-to-Moderate CO2 Concentrations on Human Decision-Making Performance». In: *Environmental Health Perspectives* 12 (Sept. 2020), pp. 1671–1677 (cit. on p. 43).